Progress in Piezo-Phototronic-Effect-Enhanced Light-Emitting Diodes and Pressure Imaging

Caofeng Pan, Mengxiao Chen, Ruomeng Yu, Qing Yang, Youfan Hu, Yan Zhang, and Zhong Lin Wang**

Wurtzite materials exhibit both semiconductor and piezoelectric properties under strains due to the non-central symmetric crystal structures. The three-way coupling of semiconductor properties, piezoelectric polarization and optical excitation in ZnO, GaN, CdS and other piezoelectric semiconductors leads to the emerging field of piezo-phototronics. This effect can efficiently manipulate the emission intensity of light-emitting diodes (LEDs) by utilizing the piezo-polarization charges created at the junction upon straining to modulate the energy band diagrams and the optoelectronic processes, such as generation, separation, recombination and/or transport of charge carriers. Starting from fundamental physics principles, recent progress in piezo-phototronic-effect-enhanced LEDs is reviewed; following their development from single-nanowire pressure-sensitive devices to high-resolution array matrices for pressure-distribution mapping applications. The piezo-phototronic effect provides a promising method to enhance the light emission of LEDs based on piezoelectric semiconductors through applying static strains, and may find perspective applications in various optoelectronic devices and integrated systems.

1. Introduction

The dynamic and adaptive interactions between micro-/nanoelectronic systems and their physical environment are essential to advancing wearable technology,[1] biomedical diagnostics,[2] robotics, smart sensor networks,[3] and advanced manufacturing.[4] It is thus crucial to develop next-generation functional devices for detection,[5] processing and controlling of information encoded in environmental stimuli.[6] Although non-electrical stimuli, such as mechanical agitations, are ubiquitous and abundant in the environment for powering and controlling the micro-/nanodevices,[7] it is not facile to directly interface mechanical stimuli with the state-of-the-art silicon (Si)-based technology that relies on electrical modulation of charge-carrier transport[8] in semiconductors.[9] The piezoelectric effect, which presents polarizations under mechanical deformation in materials without inversion symmetry, has been extensively investigated in bulk crystals, thin films and nanostructures for electromechanical sensing,[10] actuation and energy harvesting.[11] Traditional piezoelectric materials such as $Pb(Zr_xTi_{1-x})O_3$ (PZT) and poly(vinylidene fluoride) (PVDF) are almost dielectric and excluded as building blocks for functional electronics.[12] The effect of mechanical strain-induced polarization on electronic transport processes of charge carriers in piezoelectric materials has therefore been long overlooked.[13]

Recently, investigations on the three-way coupling among piezoelectric polarization, semiconductor properties and photon excitation under mechanical perturbations in wurtzite-structured semiconductors,[14] e.g., ZnO and GaN, has led to an emerging field of piezo-phototronics.[15] By exerting substantial influences on the concentration/distribution of free carriers and/or the modulation of electronic energy states at the local interface of piezoelectric semiconductors, the localized polarization charges created upon static straining can effectively modulate or control the generation, separation, transport, and recombination of photogenerated charge carriers at the vicinity of a metal–semiconductor (M–S) Schottky contact[16] or p–n junction;[17] This effect is known as the piezo-phototronic effect. Piezo-phototronics describes devices which operate with piezoelectric polarization charges as a “gate”, controlling signal to achieve tunable optoelectronic performances.[18] The piezo-phototronic effect can effectively tune the performance of solar cells, LEDs, chemical/biochemical/photosensors, electrochemical processes and catalysts.[19] Here, the fundamental physics of the piezo-phototronic theory is interpreted, and milestone advances in the development of piezo-phototronic-effect-enhanced LEDs from single-nanowire devices to high-resolution pressure-distribution mapping applications are systematically reviewed.

Prof. C. Pan, M. Chen, Y. Zhang, Prof. Z. L. Wang
Beijing Institute of Nanoenergy and Nanosystems
Chinese Academy of Sciences
Beijing 100083, P. R. China
E-mail: cfpan@binn.cas.cn; zhong.wang@mse.gatech.edu
R. Yu, Prof. Q. Yang, Prof. Y. F. Hu, Prof. Z. L. Wang
School of Materials Science and Engineering
Georgia Institute of Technology
Atlanta, Georgia 30332–0245, USA

DOI: 10.1002/adma.201503500

2. Fundamentals of Piezo-Phototronics

2.1. Piezo-Potential

Certain wurtzite materials, such as ZnO, GaN, InN, and ZnS, simultaneously possess semiconductor and piezoelectric

© 2015 WILEY-VCH Verlag GmbH & Co. KGaA, Weinheim

properties. Upon straining, piezoelectric polarization charges are induced at the two ends of the crystal along certain orientations.[20] For example, ZnO has a hexagonal structure with anisotropic properties in the directions along and perpendicular to the *c*-axis.[21] The Zn^{2+} cations and the O^{2-} anions are tetrahedrally coordinated, and the centers of positive charges and negative charges overlap with each other in the normal state. When stress is applied along the *c*-axis, a displacement between the center of cations and the center of anions occurs, thus an electrical dipole moment is induced (**Figure 1**a). As all the units in the crystal present such a dipole moment under strain, an electrical potential distribution, which is called the piezo-potential (piezoelectric potential),[22] is macroscopically produced along the straining direction (Figure 1b).[20,23] Therefore, negative piezoelectric polarization charges are present in the +*c* direction, while positive piezo-charges are induced at the –*c* direction. Piezo-potential/polarization charges form the core of piezotronics and piezo-phototronics, allowing modulation of the electronic transport properties across the local interface of an M–S contact or p–n junction under mechanical deformation.

2.2. Piezoelectric Polarization at Metal-Semiconductor Contacts

The M–S contact is the fundamental construction of semiconductor-based electronics and optoelectronics.[16,24] Devices with a Schottky contact[11d] formed between metal and semiconductors are of interest in the studies of piezo-phototronics. By contacting the metal with semiconductors, a significant redistribution of charge at the junction area occurs,[25] the Fermi levels on both sides align and the M–S system reaches thermal equilibrium.[26] Accordingly, the energy band is rebuilt to form a Schottky barrier at the local M–S interface with barrier height of $e\phi_{Bn}$. The Schottky barrier height (SBH) is a measurement of the energy band mismatch, which dominates the electric transport of charge carriers across the interface when reversely biased.[27]

The strain-induced piezoelectric polarization charges presented at the vicinity of the local Schottky contact in piezoelectric semiconductors can effectively modulate the SBH and thus tune/control the transport property of the device. Taking n-type semiconductors as an example, for simplicity, ignoring the surface states and other anomalies, at zero biased voltage, space charge distribution and the energy band diagram at the M–S contact are significantly affected by the presence of the piezoelectric polarization charges. Upon compressive straining along the *c*-axis, negative polarization charges are induced at the +*c* axis interface, which repel electrons away from the interface, resulting in a wider depletion zone and a higher SBH (**Figure 2**a). Conversely, by applying tensile strains along the *c*-axis, positive piezo-charges are created at the +*c* axis interface which attract electrons, leading to a narrower depletion zone and lower SBH (Figure 2b).[11d]

According to diffusion theory, the current flowing through the Schottky barrier can be expressed as:[28]

$$J_n \approx J_D\left[\exp\left(\frac{qV}{kT}\right)-1\right] \quad (1)$$

Caofeng Pan received his B.S. degree (2005) and his Ph.D. (2010) in Materials Science and Engineering from Tsinghua University, China. He then joined in the group of Professor Zhong Lin Wang at the Georgia Institute of Technology as a postdoctral fellow. He is currently a professor and a group leader at Beijing Institute of Nanoenergy and Nanosystems, Chinese Academy of Sciences since 2013. His main research interests focus on the fields of piezotronics/piezo-phototronics for fabricating new electronic and optoelectronic devices and self-powered nanosystems. Details can be found at http://piezotronics.binncas.cn/.

Mengxiao Chen received her B.S. in physics from Northeastern University in 2012 and is currently a Ph.D. student with Prof. Z. L. Wang at the Beijing Institute of Nanoenergy and Nanosystems, CAS. She is interested in novel self-powered systems and multifunctional photoelectric devices, and is now focused on electronic applications of piezo-phototronics

Zhong Lin (ZL) Wang is the Hightower Chair in Materials Science and Engineering, Regents' Professor, at Georgia Institute of Technology. He is also the chief scientist and director of the Beijing Institute of Nanoenergy and Nanosystems, Chinese Academy of Sciences. Prof. Wang has made original and innovative contributions to the synthesis, characterization, and fundamental physical properties of oxide nanobelts and nanowires. He is the lead figure in ZnO nanostructure research. His discovery and breakthroughs in developing nanogenerators established the principle and technological roadmap for harvesting mechanical energy from the environment and biological systems for powering personal electronics. He coined and pioneered the field of piezotronics and piezo-phototronics.

© 2015 WILEY-VCH Verlag GmbH & Co. KGaA, Weinheim
Adv. Mater. **2015**,
DOI: 10.1002/adma.201503500

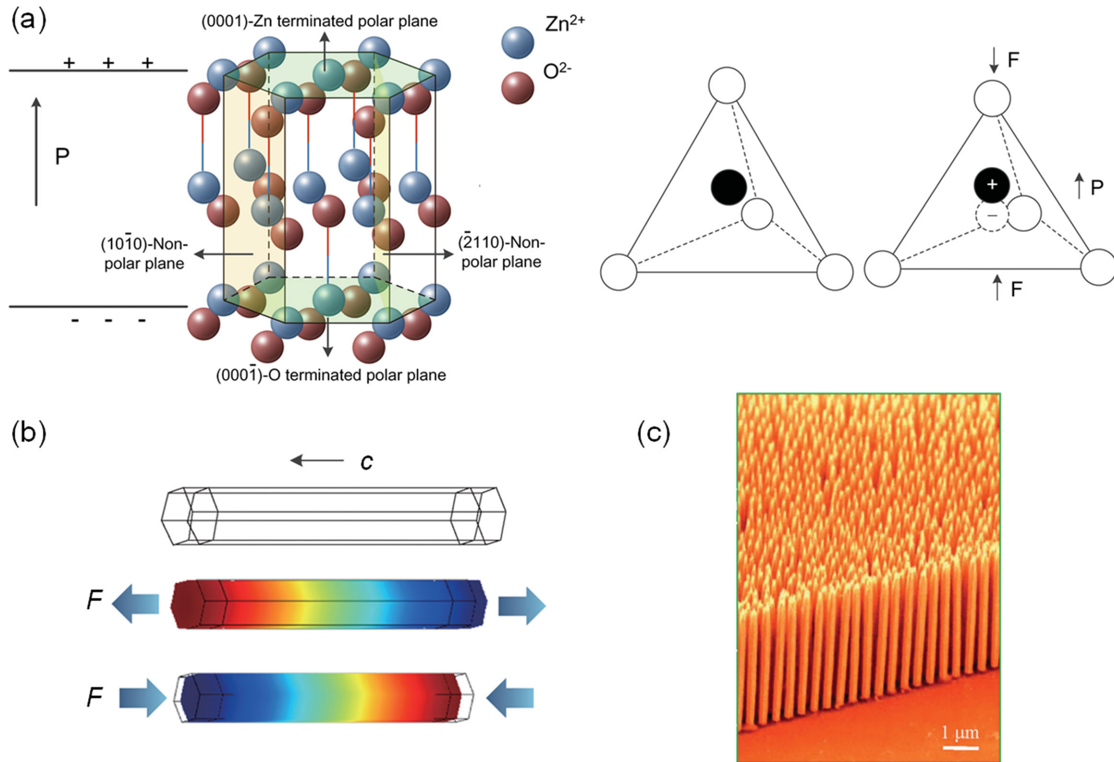

Figure 1. Piezopotential in wurtzite crystal. a) Atomic model of the wurtzite-structured ZnO. Reproduced with permission.[11a] Copyright 2012, Wiley-VCH. b) The distribution of piezopotential along a ZnO NW under axial strain calculated by numerical methods. The growth direction of the NW is along the c-axis.The color gradient represents the distribution of piezopotential in which red indicates positive piezopotential and blue indicates negative piezopotential. Reproduced with permission.[23] Copyright 2009, American Institute of Physics. c) Aligned ZnO-nanowire arrays by solution-based approach. Reproduced with permission.[19] Copyright 2012, Springer Verlag.

where: $J_D \approx q^2 D_n N_C (kT)^{-1} \sqrt{\left[2qN_D(\Psi_{bi}-V)\varepsilon_S^{-1}\right]}\left[\exp\frac{-q\phi_{Bn}}{kT}\right]$ is the saturation current density. Here, q is the carrier charge, V is the applied voltage, k is the Boltzmann constant, T is the temperature, D_n is the electron diffusion coefficient, N_C is the effective density of states in the conduction band, N_D is the donor concentration in semiconductor, Ψ_{bi} is the built-in potential, ε_S is the permittivity of the semiconductor, and ϕ_{Bn} is the SBH. The saturation current density with the absence of the piezoelectric polarization charges is:

$$J_{D0} \approx q^2 D_n N_C (kT)^{-1} \sqrt{\left[2qN_D(\Psi_{bi0}-V)\varepsilon_S^{-1}\right]}\left[\exp\frac{-q\phi_{Bn0}}{kT}\right] \quad (2)$$

where Ψ_{bi0} and ϕ_{Bn0} are the built-in potential and the SBH, respectively, with the absence of piezoelectric polarization charges. The perturbation to the conductive band edge brought on by the polarization charges is reflected by the altered SBH. This factor is further derived as:

$$\phi_{Bn} = \phi_{Bn0} - q^2 \rho_{piezo} W_{piezo}^2 (2\varepsilon_S)^{-1} \quad (3)$$

W_{piezo} is the piezoelectric polarization charge layer thickness, which is assumed to be much smaller than the width of the charge depletion zone,[29] and this layer distributes near the M–S interface. It is believed to be related to the doping concentration of the semiconductor, the strain applied on the piezoelectric material and other factors being investigated. ρ_{piezo} is the density of polarization charges. The relation between applied strain and SBH could then be described as:

$$P_Z = e_{33}s_{33} = q\rho_{piezo}W_{piezo} \quad (4)$$

In this equation, e_{33} is the piezoelectric coefficient and s_{33} is the applied strain along the polar axis of the piezoelectric semiconductor material. Consequently, the correlation between current density across the M–S interface and applied strain can be rewritten as:

$$J_n \approx J_{D0} \exp\left[qe_{33}s_{33}W_{piezo}(2\varepsilon_S kT)^{-1}\right]\exp\left[qV(kT)^{-1}-1\right] \quad (5)$$

It is clear that the charge-carrier transport is directly related to the polarity of the induced strain: when positive piezoelectric polarization charges (positive ρ_{piezo}) are induced at the local M–S contact (positive s_{33}), the transport current density increases; when negative piezoelectric polarization charges (negative ρ_{piezo}) are induced (negative s_{33}), the transport current density decreases. This is the fundamental mechanism by which transport properties are modified by piezo-polarization charges at the M–S contact.

2.3. Piezoelectric Polarization at the p–n Junction

By contacting a p-type semiconductor with a n-type one, a p–n junction is formed. This has been widely applied in

© 2015 WILEY-VCH Verlag GmbH & Co. KGaA, Weinheim

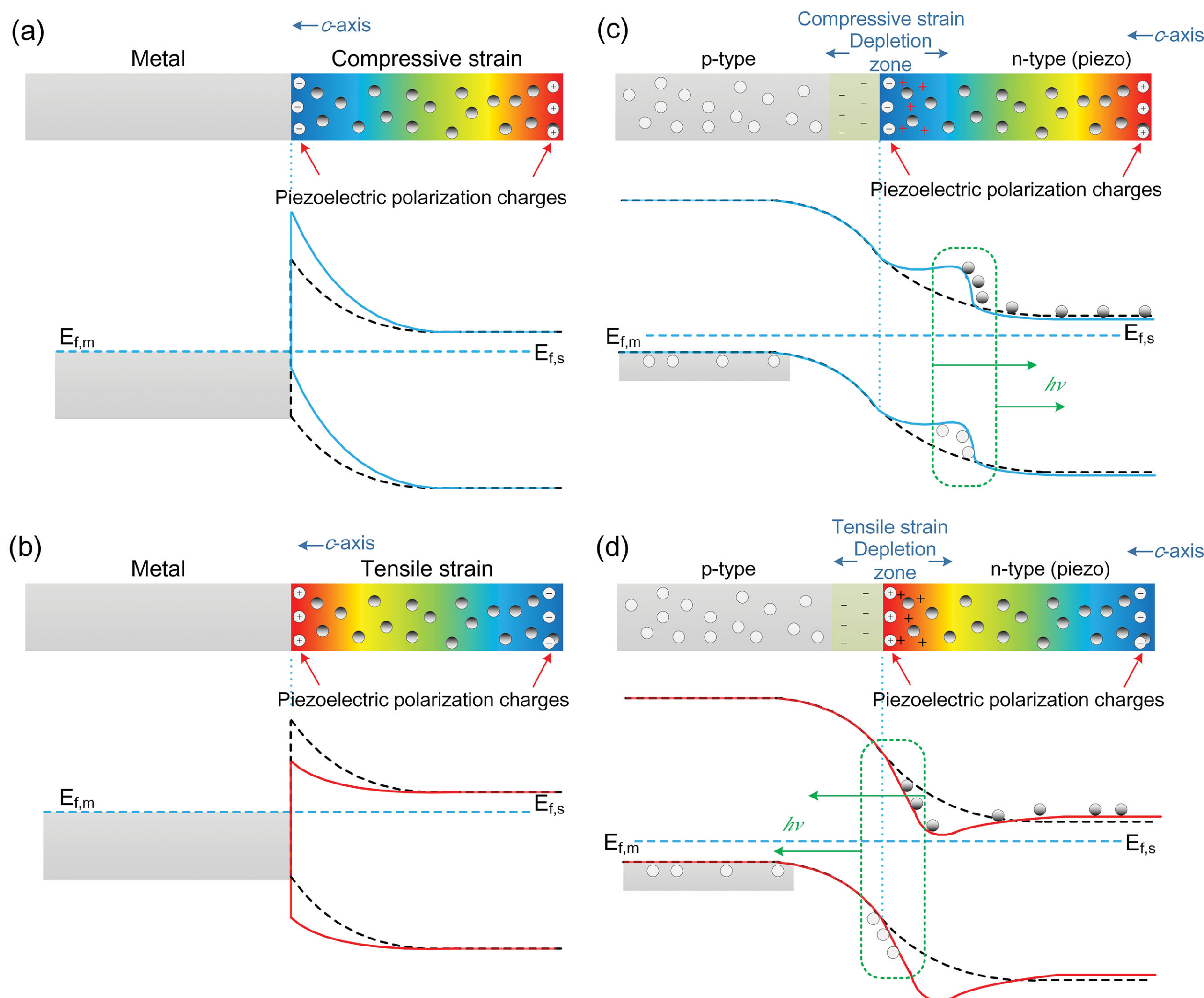

Figure 2. Schematic of the energy band diagram illustrating the piezo effect on the M–S interface and piezo-phototronic effect on p–n junction interface. a) Negative polarization charges are induced at the interface, increasing the barrier height. b) Positive polarization charges are induced at the interface, decreasing the barrier height. c) Negative polarization charges are induced at the interface, creating a bump in the band diagram. d) Positive polarization charges are induced at the interface, creating a dip in the band diagram. For the color gradient, red represents positive potential and blue represents negative potential. a–d) Reproduced with permission.[11a] Copyright 2012, Wiley-VCH.

various optoelectronic devices,[30] including LEDs,[31] solar cells[32] and photodetectors.[33] Similar to the modifications to the SBH introduced by the strain-induced piezo-charges at M–S contacts, the energy band at p–n junctions is tuned by the corresponding piezo-charges created upon straining as well,[11d] which in turn effectively control the generation, separation, recombination and transport of photo-induced charge carriers at the local hetero-/homojunction of the optoelectronic devices.[11c] This is the piezo-phototronic effect.

Here we take the homogeneous p–n junction with piezoelectricity only in the n-type semiconductor as an example. Considering typical piezoelectric semiconductors like ZnO NW,[34] by applying compressive strains along the *c*-axis, negative piezoelectric polarization charges are induced in the +*c* direction within the depletion zone, and repel electrons away from the interface. A bump in the local band structure near the interface is created in the p–n junction area (Figure 2c). If the carrier transport is mainly based on holes, this upward bending could trap more holes from the adjacent p-type material, increasing the recombination rate of carriers and number of photons generated through radiative transition in the n-side. Conversely, the tensile-strain-induced positive piezoelectric polarization charges in the n-type region attract electrons near the interface, resulting in a dip in the local band diagram as shown in Figure 2d. Accumulations of electrons appear in this downward bending, and the recombination rate of carriers and number of photons produced through radiative transition in the p-side are enhanced.[35] Therefore, certain light-emitting processes can be modulated by externally applied strains if the piezoelectric semiconductor is selected correctly.

© 2015 WILEY-VCH Verlag GmbH & Co. KGaA, Weinheim
Adv. Mater. **2015**,
DOI: 10.1002/adma.201503500

To quantitatively explain the piezo-phototronic effect on LEDs,[36] an abrupt junction model is used here. The built-in potential is given by:[17]

$$\Psi_{bi} = q(2\varepsilon_S)^{-1}\left(N_A W_{Dp}^2 + \rho_{piezo} W_{piezo}^2 + N_D W_{Dn}^2\right) \quad (6)$$

where N_A is the acceptor concentration, N_D is the donor concentration, ρ_{piezo} is the density of polarization charges, W_{Dp} and W_{Dn} are widths of depletion regions in p-type side and n-type side, respectively. W_{piezo} is the piezoelectric polarization charge layer thickness, and ε_S is the permittivity of the semiconductor. This equation suggests that the change in the built-in potential is mainly tuned by the strain-induced piezoelectric charges, thus it is the key parameter in optoelectronic applications. Similar to the regulating effect of Schottky contact, modulation can be achieved by the relative change of band diagrams in the p–n junction. We assume that $P_{n0} > N_{p0}$, where P_{n0} is the thermal equilibrium hole concentration in the n-type material, and N_{p0} is the thermal equilibrium electron concentration in the p-type material.

The total current density of a p–n junction is:

$$J_n \approx J_{C_0} \exp\left[q e_{33} s_{33} W_{piezo} (2\varepsilon_S kT)^{-1}\right] \exp\left[qV(kT)^{-1} - 1\right] \quad (7)$$

J_{C0} represents the saturation current density without piezoelectric charges. Therefore, the optical power output of a piezo-phototronic LED is obtained as:[37]

$$P_{optic} = \beta\left\{J_{C_0} \exp\left[q e_{33} s_{33} W_{piezo} (2\varepsilon_S kT)^{-1}\right] \exp\left[qV(kT)^{-1} - 1\right]\right\}^b \quad (8)$$

where β is a constant depending on device materials and structures, and b is the power-law parameter, with $b = 1$ corresponding to the linear approximation and $b \neq 1$ corresponding to the nonlinear approximation. The external quantum efficiency (EQE) is described as $\eta_{ex} = \alpha\eta_{ex0}$, where η_{ex0} is the EQE without piezoelectric charges inside the p–n junction and α is a term to measure the modulation of the piezo-phototronic effect on the carrier transport and recombination processes.

$$\alpha = \left\{\exp\left[q^2 \rho_{piezo} W_{piezo}^2 (2\varepsilon_S kT)^{-1}\right]\right\}^{b-1} \quad (9)$$

The critical parameter η_{ex} for LED, which is closely related to the luminous efficacy, can be rewritten as:

$$\eta_{ex} = \exp\left[q e_{33} s_{33} W_{piezo} (2\varepsilon_s kT)^{-1}\right]\eta_{ex0} \quad (10)$$

which clearly illustrates the control of piezo potential on the photo-emission process in the piezo-phototronic LED.

2.4. Analytical Simulation of Piezo-Phototronic Effect on LEDs

A critical concept in the strain modulation of piezo-phototronic LEDs is the rebuilding of the energy band edge at the interface, which creates either an upward bending channel or a downward bending channel in the junction area according to the strain direction.[38] These channels are effective means of controlling the carrier separation and recombination as described in the p–n junction section.[39] Here, we further confirm the existence of such channels through theoretical simulations and provide more details to guide the experimental processes.[40]

Firstly, a low-doping p-ZnO/n-ZnO homogeneous[41] junction model is built; the compressive and tensile strains are both applied in the n-type side and it is assumed that the variations of the conduction band and the valance band are identical. By utilizing the finite element analysis (FEA), deformations of energy band edges are derived by solving the Poisson equation. The 1D simulation results of conduction band deformation in an n-ZnO/p-ZnO homogeneous p–n junction under different strains on the n-type side are shown in **Figure 3**a, clearly showing the upward and downward channels. Other than the channels, another significant change in the energy band diagram is the width of the depletion region. Former discussions in strain tuned band edge deformation are mainly based on relatively high doping profile conditions, e.g., hydrothermally grown NWs with abundant defects, which means the depletion width change could be neglected when piezoelectric polarization charges are introduced. As both the density and the total amount of local depletion charges are far larger than that of the piezoelectric polarization charges, the fixed depletion region width assumption is applicable.[42] However, when the doping profile is low, the width change in depletion zone introduced by applied strains should be taken into consideration. In the depletion region, the widths between p-type side and n-type side can be approximately described as:

$$N_A W_{Dp} = N_D W_{Dn} + \rho_{piezo} W_{piezo} \quad (11)$$

Thus, when positive piezoelectric charges are introduced $(\rho_{piezo} > 0)$ by tensile strain, the depletion zone on the n-type side shrinks, and it expands on the p-type side (Figure 3b). Conversely, when negative piezoelectric charges are introduced $(\rho_{piezo} < 0)$ by compressive strain, the depletion zone on the p-type side shrinks, and it expands on the n-type side. Simulation results are visualized in 2D models as shown in Figures 3c–e. Theoretical investigations of the band rebuild process are also conducted in n-ZnO/p-GaN[43] heterogeneous p–n junctions[44] through FEA as shown in Figure 3f,g. These results clarify the piezo-phototronic effect on the piezoelectric semiconductor-based LEDs and provide general guidance for prospective experimental applications.

3. Piezo-Phototronic-Effect-Enhanced Performance of ZnO/GaN LEDs and its Applications

3.1. Enhanced Efficiency in Vertical Single-Nanowire-Based LEDs by the Piezo-phototronic Effect

Light emission from semiconductors depends on the efficiency of carrier injection, recombination, and light extraction.[45] Maintaining the injection is the key to high emission efficiency.[46] The piezo-phototronic effect acts as a tool to tune the transport, separation and recombination processes of charge

DOI: 10.1002/adma.201503500
© 2015 WILEY-VCH Verlag GmbH & Co. KGaA, Weinheim

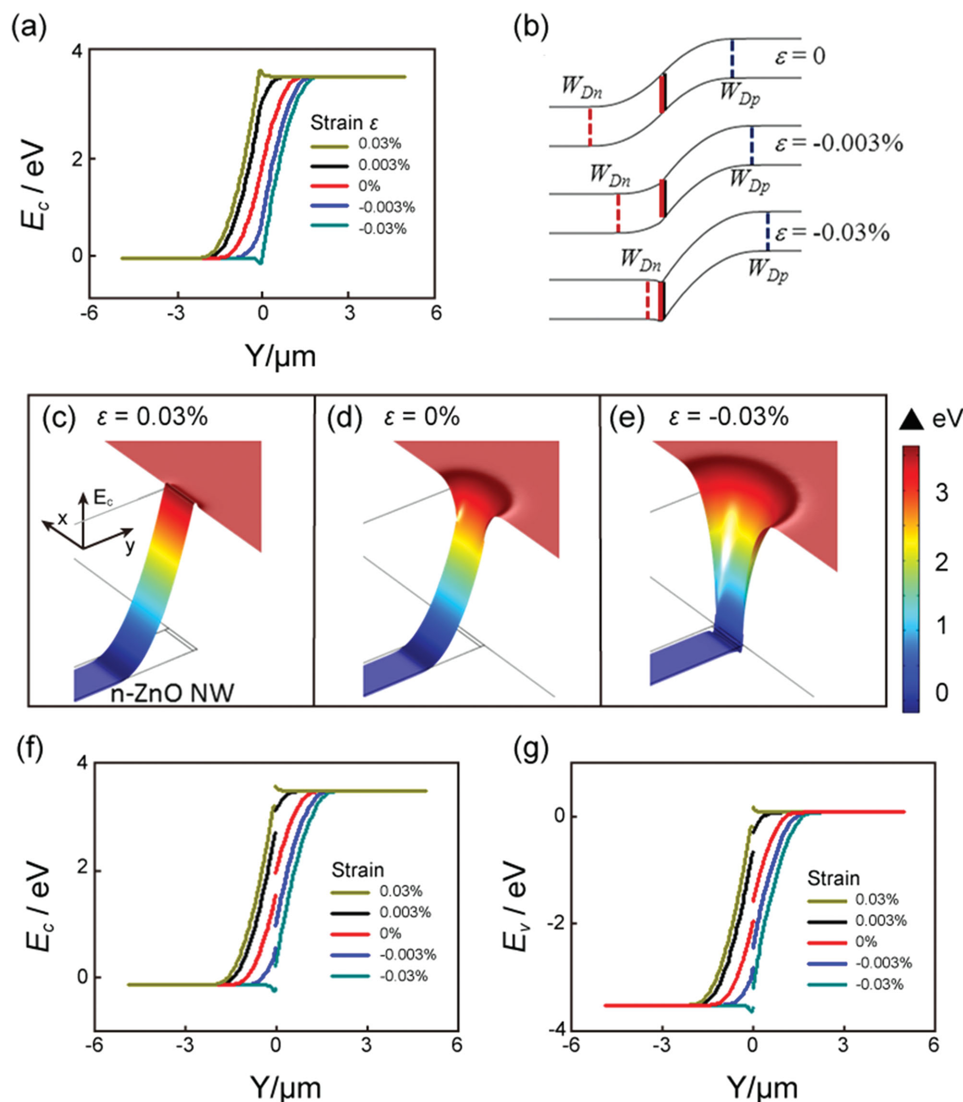

Figure 3. Simulation results for n-ZnO NW/p-ZnO and p-GaN substrate structure. a) Conduction-band deformation of the n-ZnO/p-ZnO structure under different strains on the n-type side, 1D simulation. b) Illustration of the formation of charge channel. c–e) Conduction band in height expressed from 2D simulation in the n-ZnO/p-ZnO substrate structure under: c) 0.03% strain, d) no strain, and e) −0.03% strain at the n-type side. f) Conduction-band deformation of the n-ZnO NW/p-GaN substrate structure under different strains at n-type side base on 1D simulation. g) Valence-band deformation of the n-ZnO NW/p-GaN substrate structure under different strains at the n-type side based on 1D simulation. a–g) Reproduced with permission.[40] Copyright 2014, Wiley-VCH.

carriers at the depletion area of a p–n junction, and thus is utilized to enhance the performances of LEDs.[15b] The experiment was based on a device of a single ZnO NW grown on a GaN substrate as shown in **Figure 4**a. The ZnO NW was fabricated through a hydrothermal process with the *c*-axis pointing away from the GaN thin film, and was then space filled by PMMA with its tip exposed. A layer of ITO was deposited on the top, serving as a transparent electrode,[47] and a Ni/Au electrode was used to form an Ohmic contact with the bottom p-GaN. The as fabricated device was fixed at the piezo nanopositioning stage to be observed. The optical setup is schematically illustrated in Figure 4b, which allows both CCD image capturing and spectra to be obtained. UV light was observed at the emitting end with the emission intensity increasing obviously with the compressive strains as shown in Figure 4d. The emitting light intensity was enhanced by 9 times in magnitude when applying a compressive stain of −0.149% along the *c*-axis.

The enhanced light-emission efficiency is contributed to the piezo-phototronic effect: when the ZnO nanowire is under a *c*-axis compressive strain, the strain inside the nanowire is much larger than that in the GaN thin film, so a piezo potential is introduced along the nanowire.[48] There exists a band structure deformation in the junction area, and a dip is created at the interface (Figure 4c). The distorted band structure helps to trap holes from the p-type side, and thus increases the carrier injection rates. Subsequently, the recombination efficiency of carriers increases, more photons are produced in this process and the light emission is therefore enhanced.

© 2015 WILEY-VCH Verlag GmbH & Co. KGaA, Weinheim
Adv. Mater. 2015,
DOI: 10.1002/adma.201503500

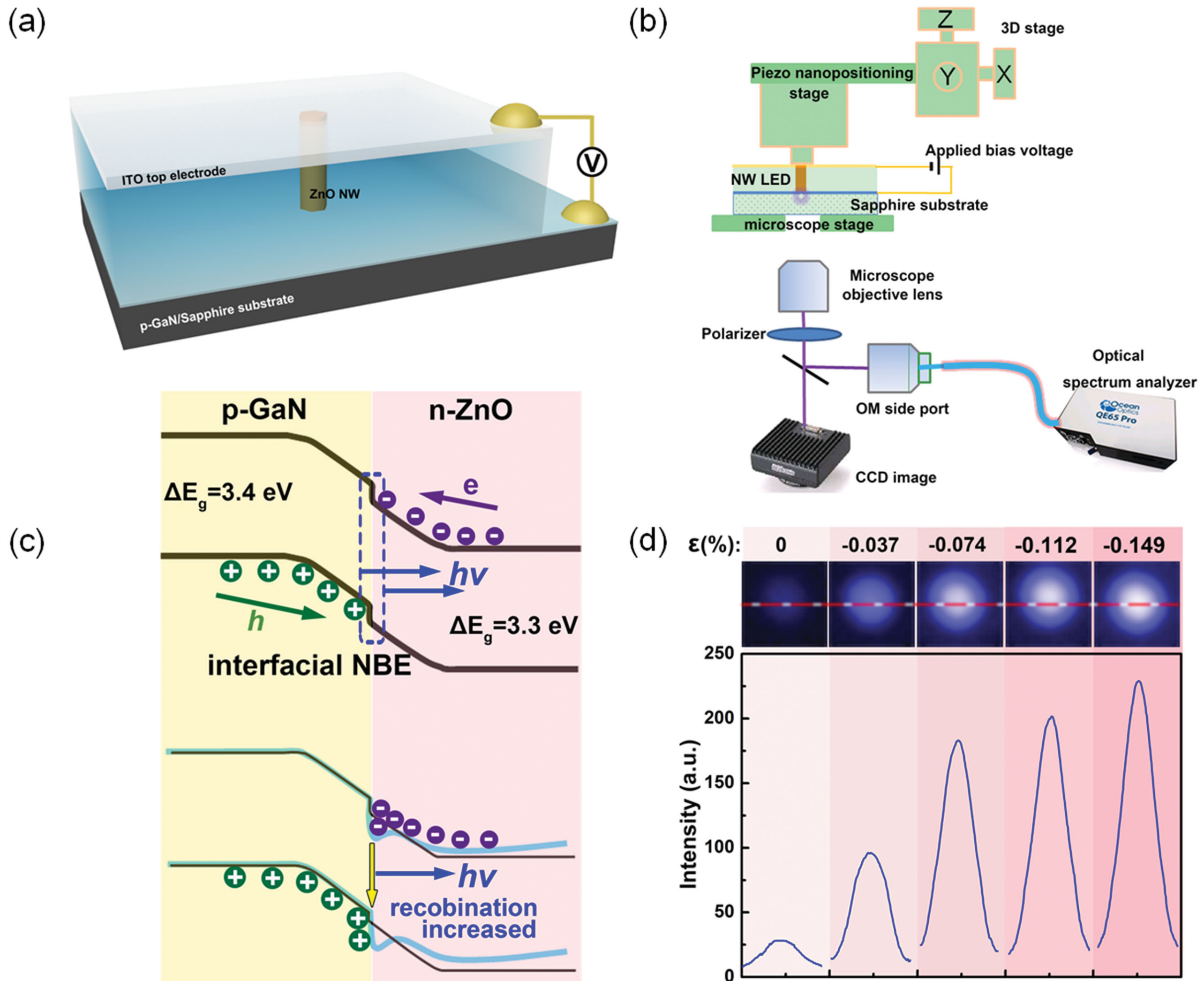

Figure 4. Vertical single-wire n-ZnO NW/p-GaN substrate LED device. a) Schematic of the packed p-GaN/n-ZnO single-wire LED. b) Design of the optical setup. c) Energy band structure of the p–n junction and band deformation of the n-ZnO NW/p-GaN substrate under compressive strains. d) CCD images recorded from the single-wire LED under different applied strains and the corresponding light intensities.

3.2. Ordered-Nanowire-Array Blue/Near UV LEDs

ZnO-based light-emitting diodes (LEDs) have been considered as potential candidates for next generation blue/near-UV light sources,[49] due to the direct wide bandgap energy of 3.37 eV, a large exciton binding energy of 60 meV at room temperature, and several other manufacturing advantages.[50] Among all the reported ZnO-based LEDs, ZnO/GaN heterojunction structured LEDs are most investigated due to the similar crystallographic structures of two materials and their suitable semiconductor properties. A single-nanowire device has been previously achieved; however, the scale limits its applications in high-performance optoelectronic devices.[51] Thus, n-ZnO nanowire/p-GaN thin film heterostructures are utilized to fabricate ordered nanowire array LEDs, which possess an external quantum efficiency of 2.5%.[52]

The design of the LED is shown in **Figure 5**a. Ordered ZnO nanowire arrays were grown on p-GaN thin film substrate (Figure 5b) with low temperature wet chemical methods and electron beam lithography (EBL). After wrapping the nanowire arrays with PMMA, and exposing the tips of the nanowires, Ohmic contacts were made to both the bottom p-GaN thin film and top n-ZnO nanowires. Then, the as-fabricated LED device was illuminated, and the optical image is shown in Figure 5c at a 10 V bias voltage. Each single nanowire operates as an LED, and the whole LED array is connected in parallel. The interval distance between each lighting spot is 4 μm and the spatial resolution is 6350 dpi. Electroluminescence spectra (Figure 5d) were obtained at different bias voltages, and peak-deconvolution with Gaussian functions was conducted to analyze the mechanism for the light emission. The inset in Figure 5d shows that there are three distinct bands centered in the range of 395–415 nm, 420–440 nm, and 450–510 nm which correspond to different recombination/emission processes. The near UV emission band centered at 400 nm is mainly from the near band edge (NBE) emission in ZnO nanowires, which is generated from

© 2015 WILEY-VCH Verlag GmbH & Co. KGaA, Weinheim

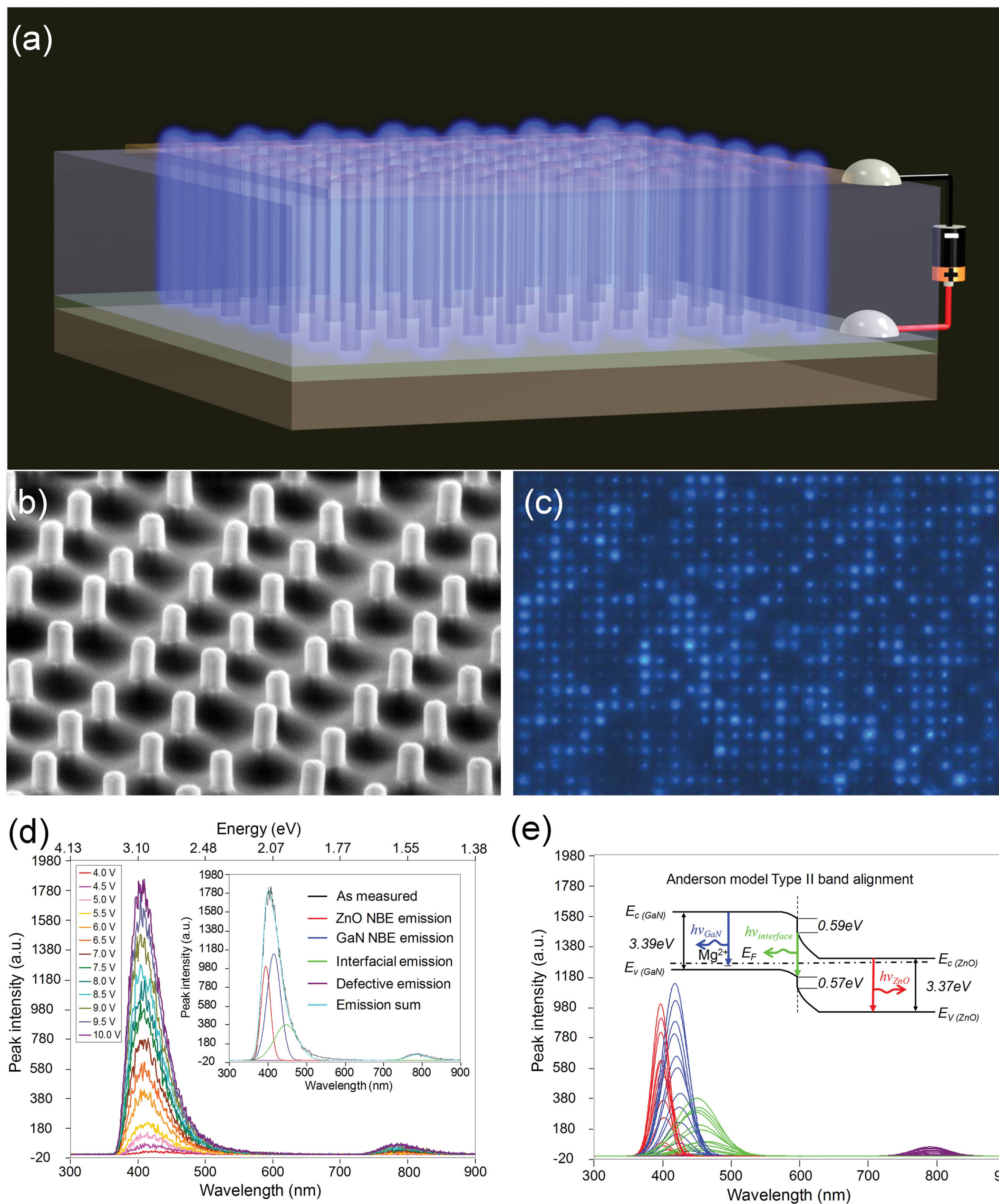

Figure 5. Ordered nanowire array of n-ZnO NW/p-GaN substrate LEDs. a) Design overview of the LED. b) 60°-tilt SEM view of the as-grown patterned vertical ZnO nanowires after they are coated with SiO_2 and wrapped with PMMA, and the tips are exposed. c) Optical image of a turned on LED (artificial bluish color). d) EL spectrum as a function of forward-bias voltage. Inset shows by Gaussian deconvolution analysis the blue/near-UV emission could be decomposed into three distinct bands that correspond to three different optoelectronic processes. e) All of the four emission bands evolve (band width, height, and intensity) as a function of the bias voltage. The inset schematics show the band diagram of the n-ZnO/p-GaN heterojunction under no or small bias voltage, where the three emission bands comprising the blue/near UV light are specifically indicated in different colors. a–e) Reproduced with permission.[52] Copyright 2010, Wiley-VCH.

© 2015 WILEY-VCH Verlag GmbH & Co. KGaA, Weinheim
Adv. Mater. **2015**,
DOI: 10.1002/adma.201503500

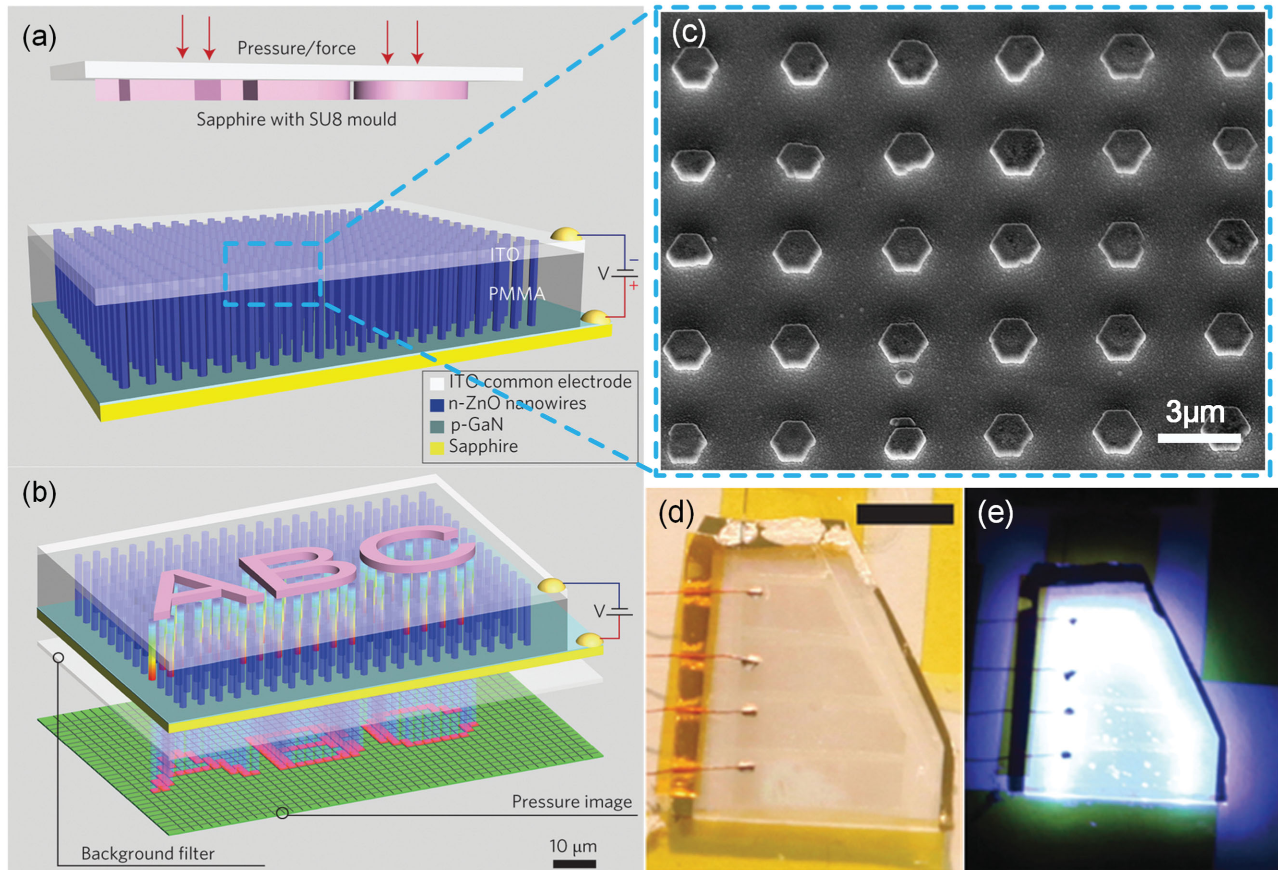

Figure 6. n-ZnO NW/p-GaN substrate nanowire LED array for electroluminescent imaging of a pressure distribution. a,b) Design of the NW-LED-based pressure-sensor array before and after applying a compressive strain. c) SEM images of the as-grown ZnO NW arrays on the p-GaN film with PMMA wrapping around the nanowires and an ITO layer deposited as a common electrode on top of the n-ZnO NWs. d,e) Optical image of a fabricated device and corresponding image when the device was electrically lit up at a bias voltage of 5 V, showing blue-white light emission from the NW-LED array. The scale bar is 5 mm. a–e) Reproduced with permission.[57] Copyright 2013, Macmillan Publishers Limited.

the recombination of ZnO free and bound excitons,[53] whereas the emission band centered at ca. 430 nm is attributed to the transitions from the conduction band or shallow donors to deep Mg acceptor levels in the p-GaN.[53,54] The blue emission around 460 nm comes from the radiative recombination of the electrons from n-type side and holes from p-type side at the interfaces.[53a,55] The weak red emission at around 790 nm is ascribed to the native deep level point defects (oxygen vacancies and zinc interstitials) in ZnO nanowires.[53b] Combination of EBL and low temperature wet chemical methods realizes the ordered arrays of n-ZnO nanowires synthesized on a p-GaN thin film substrate, and achieves the blue/near-UV LEDs with controllable spatial resolutions simultaneously.

3.3. Piezo-Phototronic Nanowire LED Arrays for Electroluminescent Imaging of a Pressure Distribution

As reviewed in the previous sections, the light emission of piezoelectric semiconductor-based LEDs are modulated by the piezo-phototronic effect.[56] Since the light emission intensity is sensitive to externally applied strains, a light-based pressure sensor is developed based on a nanowire LED array. Moreover, two-dimensional (2D) pressure-distribution mapping is achieved by such devices based on the correlation between the magnitude of pressure applied on the LEDs and the intensity of light emitted from them.[57] This work indicates promising applications of such devices for human-machine interface,[58] visualized pressure-mapping system and smart sensor networks[59] in the future.

The structure design is illustrated in **Figure 6**a,b. The growth of the ordered ZnO nanowires was carried out through conjunction of photolithography patterning and low-temperature wet chemical methods, with the *c*-axis pointing away from the GaN thin film grown on a sapphire substrate. The nanowires were then wrapped by PMMA, which acted as both a buffering material and an insulating material, with their tips exposed through oxygen plasma etching (Figure 6c). Ni/Au bottom electrodes were fabricated to form an Ohmic contact with GaN thin film, and an ITO layer was deposited on ZnO nanowires as a top electrode. The LED device was illuminated at a bias voltage of 5V, showing the blue-white emission (Figure 6e), compared to the corresponding optical image without electrically lighting (Figure 6d). The dominant blue/near UV emission is ascribed to the near band edge (NBE) emission in ZnO nanowires, and the corresponding theoretical models for the light-emitting

© 2015 WILEY-VCH Verlag GmbH & Co. KGaA, Weinheim

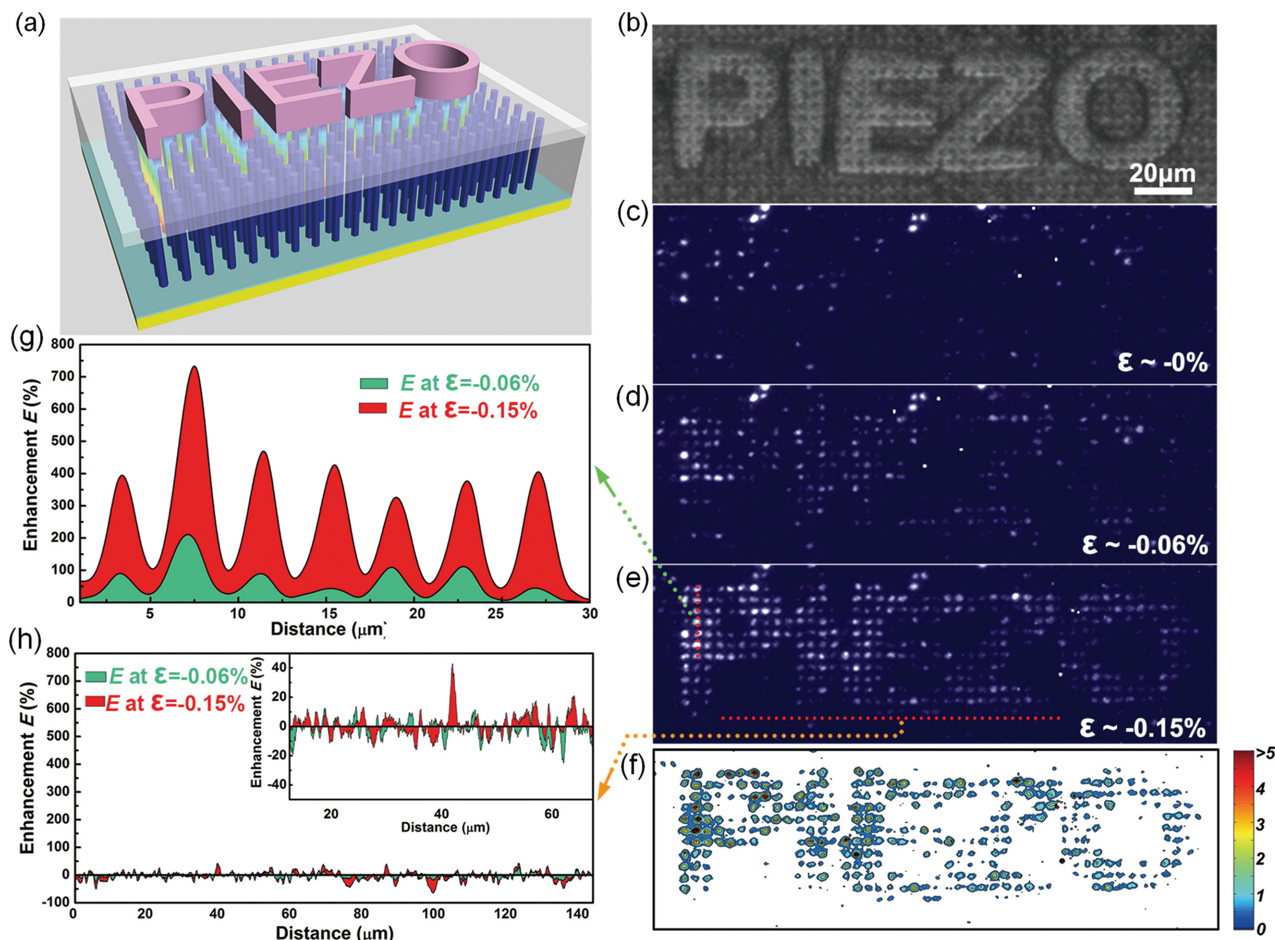

Figure 7. High-resolution parallel imaging of pressure/force distribution. a) Illustration showing the working process of pressure-distribution imaging. b) Optical image of the device with a convex mold on top. c–e) Electroluminescence images of the device at strains of 0, –0.06%, and –0.15%, respectively. The images clearly show that a change in LED intensity occurred at the pixels that were compressed, while those away from the molded pattern showed almost no change. f) 2D contour map of the $E(x,y)$ factor derived from the LED intensity images shown in (c) and (e). It directly presents the word "PIEZO", as given on the mold. g,h) Line profile data showing the signal-to-noise ratio of the E factor for two typical positions: one on the molded pattern (vertical pink line, g) and one off the pattern (horizontal red line, h), showing unambiguous differences. a–f) Reproduced with permission.[57] Copyright 2013, Macmillan Publishers Limited.

process have been described in detail in Section 3.2. To briefly summarize them, light emission mainly comes from two processes: transition between shallow donor and deep acceptor levels in p-GaN, and combinations of electrons from n-type side and holes from p-type side at the interfaces.

The 2D strain mapping was carried out by applying pressure through a module with a convex character pattern of "piezo" on the top of the NWs array, which was fabricated with SU 8 photoresist on the sapphire substrate. **Figure 7**a shows the schematic for the pressure-mapping method and Figure 7b presents an optical image with the convex character pattern at the top. The optical image when the LED array was illuminated at a bias voltage of 5 V without applied strain is shown in Figure 7c. Pressure corresponding to a compressive strain of –0.06% was applied on the illuminated device and the optical image was recorded by a CCD camera as shown in Figure 7d. An increasing pressure up to –0.15% was further applied and the result was obtained in Figure 7e. It is obvious that the light intensity of the "piezo" pattern, became clearer as the strain increased. From the images, it can be found that LED intensity changes occurred at pixels being compressed by the patterned mold, while pixels not affected by the mold showed almost no change in light intensity. In order to have a quantitative understanding and analysis of the mapping performance, we define the enhancement factor $E(x,y) = [I\varepsilon(x,y) - I_0(x,y)]/I_0(x,y)$, where (x,y) stands for the two-dimensional coordinate of a pixel in the plane. The spatial strain distribution can be extracted from above images and visualized as Figure 7e. Choosing LED pixels on the mold (with pressure applied) as indicated by the vertical red line, the enhancement factor under a –0.15% strain (≈750%) is about 4–5 times larger than that of under a –0.06% strain (Figure 7g). This shows a high signal-to-noise ratio, while enhancement factors for the pixels outside the mold (the horizontal red line) keep at noise levels and show a random signal-to-noise ratio (Figure 7h) The comparison unambiguously shows the modulation of piezo-phototronic effect on the light emission. It proves the principle to use piezo-phototronic effect for 2D pressure-distribution mapping at a high resolution is

© 2015 WILEY-VCH Verlag GmbH & Co. KGaA, Weinheim

DOI: 10.1002/adma.201503500

achievable. From Figure 7g, we can see that the actual resolution is 2.7 μm, defined as the full-width at half maximum of the emission pixels. The center to center distance between adjacent lighting pixels is 4 μm, corresponding to a resolution of 6530 dpi, which is hardly achieved by other electronic pressure-sensing device.[60]

The devices demonstrated above are fundamentally new in science and offer a novel approach to visualize the strain distributions through LED imaging. This piezo-phototronic NW-LED sensor array features[61] fast response and ultrahigh spatial resolution. Furthermore, photoluminescence pressure-distribution mapping has also been achieved based on this structure.[62] By integrating the output light signals with advancing optical components and on-chip fabrications, this technology may be developed into highly intelligent human-machine interface solutions.

4. Piezo-Phototronic-Effect-Enhanced Performance of Inorganic/Organic Hybrid LEDs and their Applications

4.1. Enhanced Efficiency in Single-Wire ZnO/PEDOT LED by the Piezo-Phototronic Effect

The efficiency of a LED device depends on the current injection, which is dominated by the carrier (electrons and holes) generation, separation and recombination processes. However, it is usually difficult to balance the number of injected electrons and holes in heterojunction LEDs due to the different material properties and band alignment, and thus it is challenging to achieve high emission efficiency. Such difficulties are universal to both inorganic and organic[63] LEDs. Based on the investigations above, the piezo-phototronic effect provides a promising approach to improve the general performances and enhance the emission efficiency of LEDs. Therefore, a single ZnO nanowire/p-polymer core–shell structured LED is designed based on this fundamental.[64]

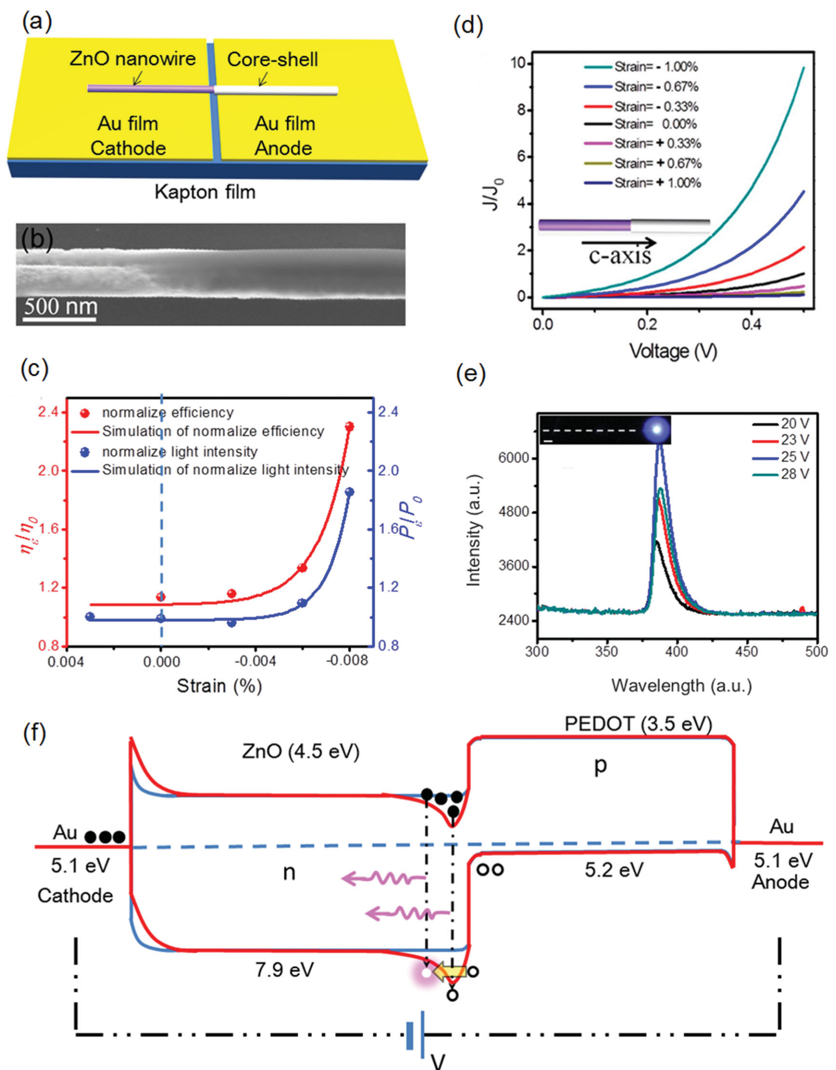

Figure 8. Inorganic/organic single-nanowire LED device. a,b) Schematic diagram and SEM image of a ZnO NW/PEDOT:PSS core–shell structure. c) Results for numerical simulation of a ZnO NW/p-polymer core–shell UV LED: Simulated current–voltage characteristics under different strains with the *c*-axis pointing away from the p-polymer. d) Change in relative light intensity $P\varepsilon/P_0$ and external efficiency $\eta\varepsilon/\eta_0$ under different strains. e) EL spectrum as a function of the forward bias voltage. f) Proposed mechanism of the enhanced light emission under strain for a ZnO NW/p-polymer core–shell UV LED under different strains. The red line represents the band diagram considering piezo-phototronic effect, while the blue line represents the case without considering the piezo-phototronic effect. a–d) Reproduced with permission.[64] Copyright 2013, American Chemical Society.

Figure 8a shows the structure design schematic and SEM image of the ZnO nanowire/PEDOT:PSS core–shell structure, indicating an excellent contact and good interface formed between these two materials. A Kapton film was packed as a substrate in order to get the characteristics under applied strains. A gap was designed as a tip to avoid short current during the fabrication of the electrodes (for detailed fabrication methods see ref. [61]. Numerical simulation was first conducted to determine the strain-induced properties of this device (Figure 8b). When the *c*-axis of the ZnO NW was pointing away from the p-polymer, the simulated *I*–*V* curves showed that the current increased with the increasing compressive strain, and decreased with increasing tensile strain. This was further confirmed by experimental results shown in Figure 8c, which revealed changes in relative light intensity, $P\varepsilon/P_0$, and external efficiency, $\eta\varepsilon/\eta_0$, under different strains. Consequently, the light emission intensity and external quantum efficiency (EQE) of the hybrid LED have been enhanced by 190% and 230%, respectively, under a −0.008% compressive strain. Seen from the electroluminescence spectra presented in Figure 8d, the

© 2015 WILEY-VCH Verlag GmbH & Co. KGaA, Weinheim

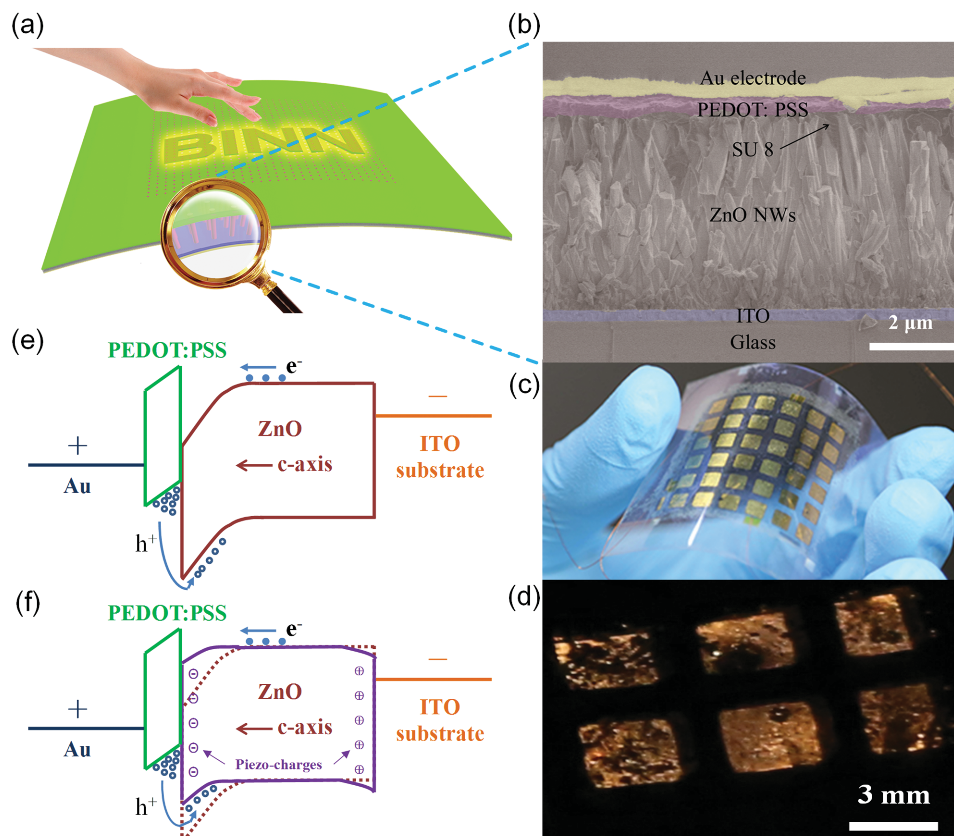

Figure 9. The flexible ZnO NW/p-polymer LED array working as a pressure-distribution sensor. a) Schematic illustration of the NW-LED-based pressure-sensor array for imaging pressure distributions. b) Cross-sectional SEM image of the ZnO nanowire/p-polymer LEDs device (false color for a better identification). c,d) Photograph of the ZnO nanowire/p-polymer LEDs based on flexible substrate and corresponding optical image when the device was electrically lit up. e,f) Energy band diagrams to illustrate the piezo-phototronic effect on the carrier recombination when the compressive strain is applied. a–f) Reproduced with permission.[70] Copyright 2015, Wiley-VCH.

light emission is localized near the end surface of the NW. The schematic band diagram of the heterostructure without strain (Figure 8e) shows that the barrier for hole injection from PEDOT:PSS into ZnO is high and limits the recombination rate. The majority of electrons flow through the interface without sufficient recombination with holes. When a compressive strain is applied with a forward bias voltage, the local negative piezo-charges increase the SBH at the cathode, and the local positive piezo-charges create a dip at the interface in the junction zone.[61c,65] It is an efficient method to increase the carrier recombination rate. Subsequently, the EQE of the hybrid LED and light emission intensity are enhanced.

4.2. Flexible and Controllable Piezo-Phototronic LED Arrays as Pressure-Mapping Sensor Matrices

Functional tactile sensing devices for high-resolution pressure-distribution mapping have been achieved by array devices based on n-ZnO NWs/p-GaN heterojunctions.[57] To improve the flexibility and adaptability of such devices, PEDOT: PSS and patterned ZnO NWs have been assembled to fabricate flexible[66] LED arrays as pressure-mapping systems.[67] **Figure 9**a shows the structure design of such an n-ZnO NW/PEDOT: PSS LEDs array device.[68] The device was fabricated based on a patterned array of n-ZnO NWs synthesized on an ITO/PET substrate, with the *c*-axis pointing away from the substrate. After infiltrating the between-nanowire space with SU-8 and spin-coating a layer of PEDOT:PSS,[69] an Au layer was deposited on top of the PEDOT:PSS to form a common electrode.[70] Detailed planar structures of a ZnO NW/p-polymer LEDs device are clearly characterized by the cross-section SEM image as shown in Figure 9b. The corresponding optical images of a flexible pressure-mapping device are presented in Figure 9c. When the device was illuminated at room temperature, yellow light was observed (Figure 9d), which is associated with the non-perfect crystallinity and high defect concentrations of ZnO nanowire synthesized through the low-temperature hydrothermal method. The band diagrams in Figure 9e,f show how the piezo-phototronic effect regulates the carrier recombination when the compressive strain is applied.

The piezo-phototronic effect on the device was investigated by pressing a convex-character pattern of "BINNmade of SU8 (Figure 9a).The enhancement performance is determined by actual compressive strains applied on individual ZnO NWs. Thus, the sensitive ranges differ for devices with different NWs geometries in certain pixels. We define the sensitivity S[71] by Equation (12):

© 2015 WILEY-VCH Verlag GmbH & Co. KGaA, Weinheim

DOI: 10.1002/adma.201503500

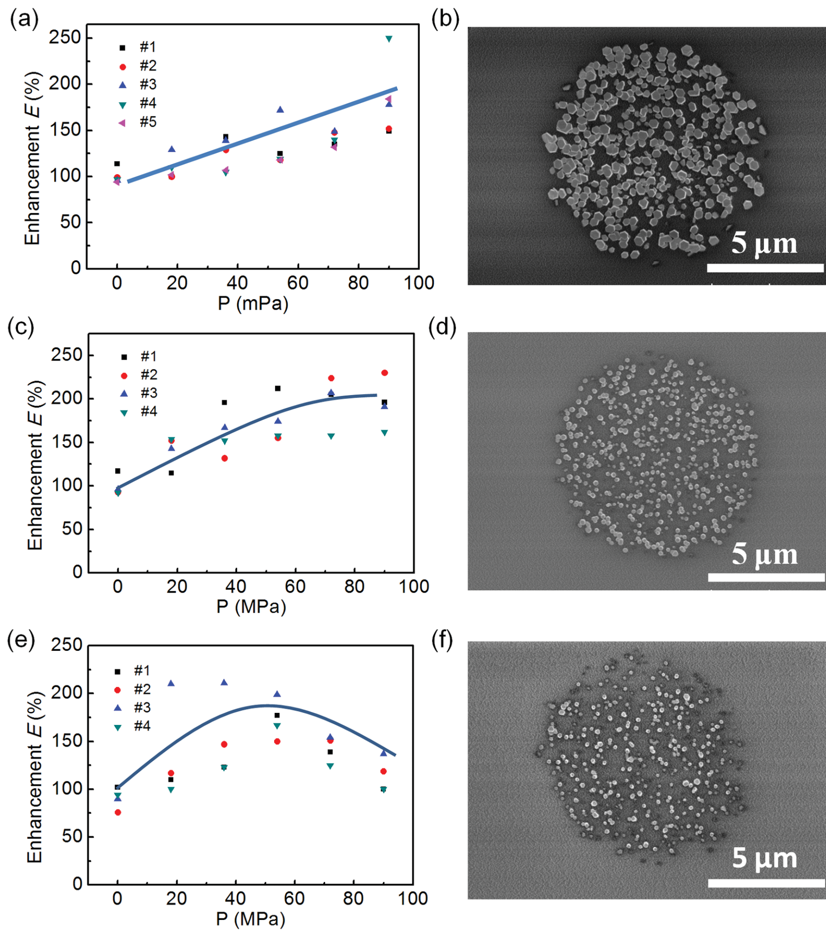

Figure 10. Light-intensity enhancement of device with different NW geometries under the same external pressures. a,c,e) Enhancement factor E of an NW-LED as a function of the applied pressure with the ZnO NWs synthesized in: a) 80×10^{-3} M, c) 60×10^{-3} M, and e) 40×10^{-3} M nutrient solution. b,d,f) The corresponding SEM images of ZnO NWs synthesized in: b) 80×10^{-3} M ($\Delta a \approx 25\%\ a$), d) 60×10^{-3} M ($\Delta a \approx 15\%\ a$), and f) 40×10^{-3} M ($\Delta a \approx 8\%\ a$) nutrient solution. a–f) Reproduced with permission.[70] Copyright 2015, Wiley-VCH.

$$S = \frac{\Delta I / I_0}{\sigma} = \frac{E-1}{\sigma} \tag{12}$$

where E is the enhancement factor, $\Delta I = I_p - I_0$ and σ is the pressure applied to each ZnO NW. Considering each pixel is composed of numerous ZnO NWs, then $\sigma = \frac{P}{\Delta a / a}$, in which P is the pressure applied to the whole device, a is the total area of the pixel (i.e., a square), while Δa is the area of ZnO NWs with head exposed in each pixel. **Figure 10**b,d,f show different geometries (length, diameter and density of ZnO NWs) from different concentrations of nutrient solution (from 40×10^{-3} M to 80×10^{-3} M), and corresponding enhancement performances are shown in Figure 10a,c,e. We can see that the sensitive range for devices with ZnO NWs synthesized in 80×10^{-3} M nutrient solutions is up to 100 MPa (Figure 10a), while for devices with ZnO NWs synthesized in 40×10^{-3} M nutrient solutions it is limited to less than 50 MPa (Figure 10e). Therefore, according to the actual application requirement, the pressure-measurement range of the LED mapping system can be controlled varying from 40 to 100 MPa by changing the growth conditions of the ZnO NWs array. Combining strain sensitive piezoelectric material with flexible organic/inorganic[72] hybridized LED technology will bring numerous potential applications to human–machine interfaces.[71]

5. Enhancing Light Emission of Silicon-Based Heterostructure Arrays by the Piezo-Phototronic Effect

As silicon technology has the most well-developed manufacturing procedure in modern electronics, to integrate silicon material with optoelectronics is of great importance.[73] However, due to its indirect band gap and low carrier mobility, Si is not the best choice for large-scale integrated LEDs with high performances.[74] Considering the enhanced performance due to the piezo-phototronic effect in piezoelectric-materials-based optoelectronics, a Si-piezoelectric material[75] LED array has been fabricated based on ordered Si–micropillar array–ZnO nanofilm heterostructure.[76]

The structure design and fabrication process are shown in **Figure 11**a. The p-doped silicon wafer is the substrate material for the ordered micropillar array derived from lithography and inductive coupled plasma (ICP) etching. The n-type semiconductor is the ZnO nanofilm deposited through magnetron sputtering. Two layers of Au electrode were fabricated on the top: the sub-layer to form an Ohmic contact with the ZnO nanofilm and the up-layer to strengthen the electro-conductivity with a netlike pattern or a bar-type pattern; silver paste was used as the bottom electrode also to form an Ohmic contact with p-silicon side. The uniformity of the etched silicon micropillars, as demonstrated in Figure 11d is well ordered, with a pillar height of 5 µm, the bottom diameter of 4.1 µm and the top diameter of 1.7 µm. The ZnO nanofilm layer which is characterized in Figure 11e completely covers the Si pillars.

Each heterojunction composed of a ZnO nanofilm and a Si pillar acts as an individual light emitter, and all the pillars are connected in parallel. Thus, when the heterostructure array is illuminated by forward biased voltage, a corresponding lighting pixel matrix is observed (Figure 11b,c). The center-to-center distance between two adjacent LEDs is obtained as 5.2 µm, which is in agreement with the characterization in the fabrication process, equivalent to a pixel resolution of 4885 dpi. The actual resolution (an important parameter in LED display) is 2.6 µm, as defined by the full-width at half-maximum (FWHM) of the emission pixels. Another typical property, the electroluminescence (EL) emission spectra, were

© 2015 WILEY-VCH Verlag GmbH & Co. KGaA, Weinheim

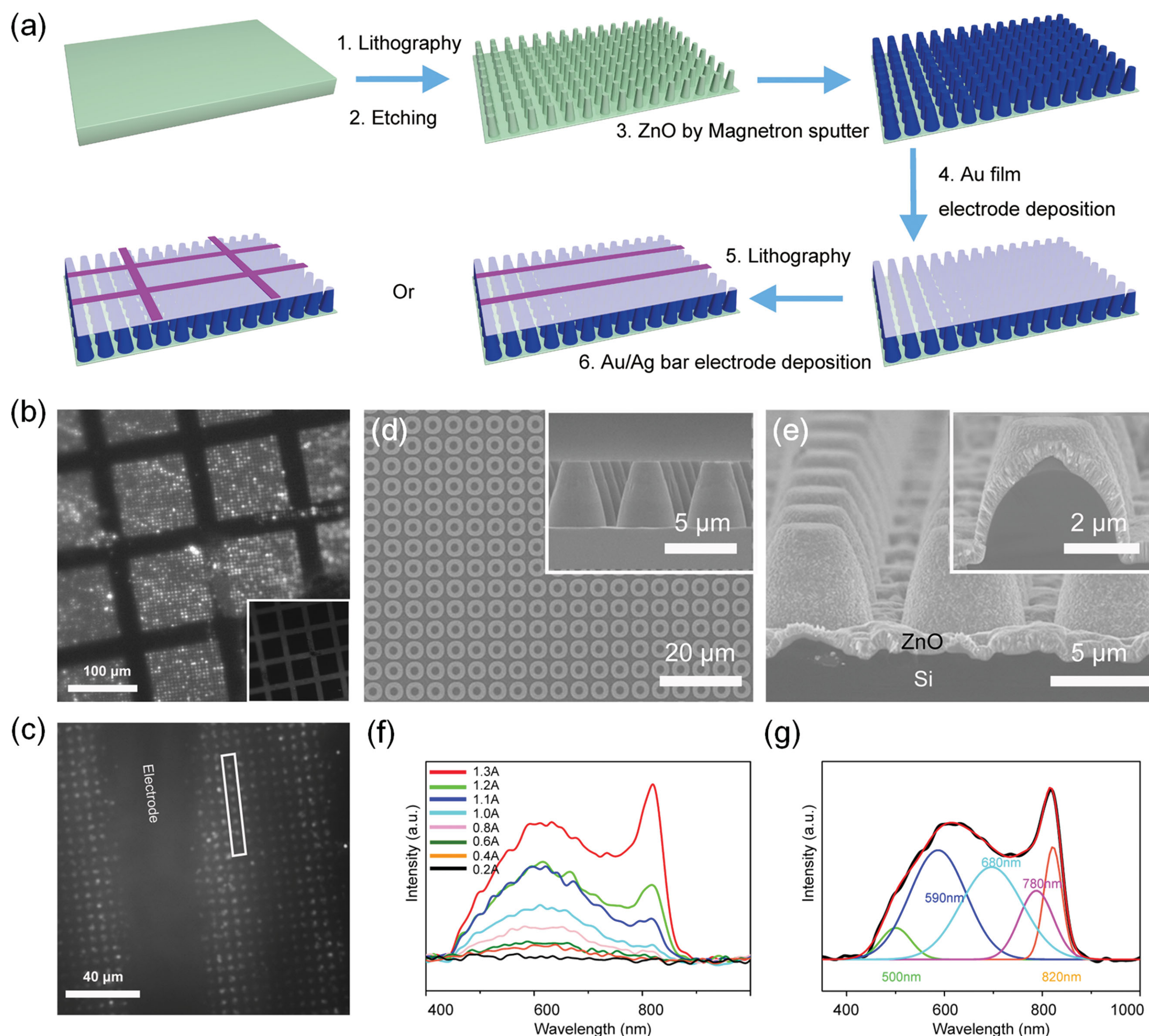

Figure 11. Structure design and optical performance of the ZnO-nanofilm/Si-micropillars LED array. a) Schematic procedures in fabricating the ZnO-nanofilm/Si-micropillars LED array. b,c) Optical images of the as-fabricated device with network electrodes and bar electrodes operating under 10 V bias voltage. d) Structure characterizations of ZSH LEDs array: top view and side view (inset) SEM images of Si micropillars. e) Cross-sectional SEM images of ZnO covered Si micropillars. f) Electroluminescence property of the device operating under different injection currents at room temperature. g) Peak deconvolution of the broad spectrum with Gaussian functions at the injection current of 1.3 A. a–g) Reproduced with permission.[76] Copyright 2015, Wiley-VCH.

obtained under a series of forward biased currents, as shown in Figure 11f. To have a better understanding of the emission spectra, we make a peak deconvolution based on Gaussian functions, and five distinct bands are derived, among which each emission band corresponds to a particular recombination process (Figure 11g).

A similar system as mentioned in the former section was utilized to apply pressure on the device and obtain the corresponding optical change. The typical *I–V* characteristics (**Figure 12**a,b) under different applied compressive strains indicate the light emission enhancement in this silicon-based-heterojunction-structured LED matrix. Moreover, the light intensity change under external applied strains shown in Figure 12c confirms the enhancement. If we define the enhancing factor of LED intensity E as $E = (I\varepsilon - I_0)/I_0$, obviously, E is approximately in linear relation with external strains, with the maximum value of 120% at a compressive strain of −0.05%. As the *c*-axis of the nanofilm is pointing away from the interface with the Si micropillar, positive piezoelectric charges are introduced when compressive strain is applied. Thus a bump in the energy diagram edge at the interface between ZnO and microsilicon is introduced, and acts as a trap for electrons, which enhances the recombination of carriers and the light emission process (Figure 12d–f).

© 2015 WILEY-VCH Verlag GmbH & Co. KGaA, Weinheim
Adv. Mater. **2015**, DOI: 10.1002/adma.201503500

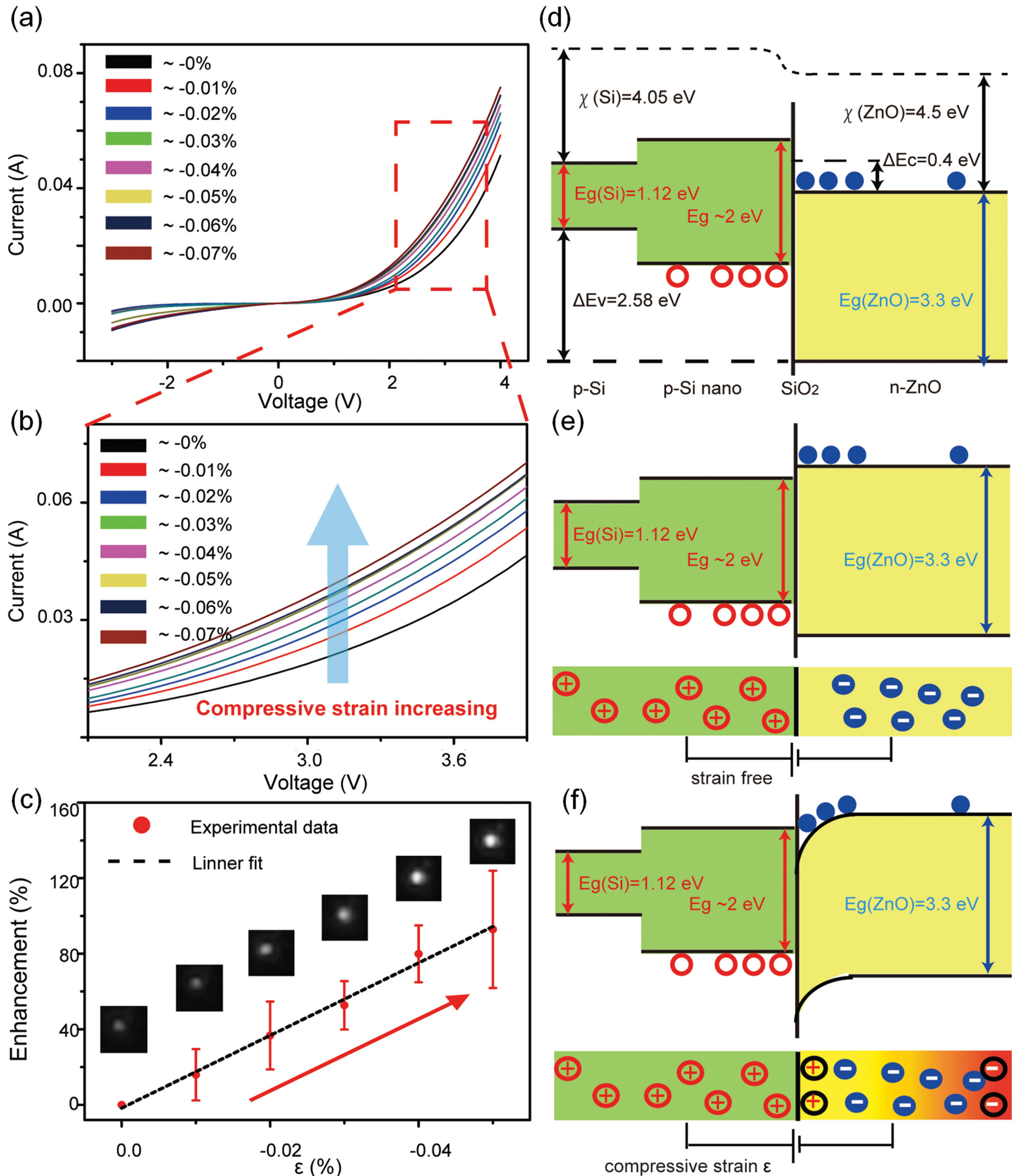

Figure 12. Piezo-phototronic effect enhancements and working mechanism for the ZnO-nanofilm/Si-micropillars LED. a,b) *I–V* characteristics of the device operating under various applied strains. c) Enhancement factor *E* vs strains *ε*, together with the corresponding images of light emissions. d–f) Energy band diagrams of ZSH LEDs array under: d) no strains nor bias voltage; e) no strain and a bias voltage; f) compressive strains and a bias voltage. a–f) Reproduced with permission.[76] Copyright 2015, Wiley-VCH.

These results indicate a promising approach to fabricate Si-based light-emitting components[77] with high performances enhanced by the piezo-phototronic effect, and make a major step towards on-chip recording of mechanical signals by optical means, with potential applications in touchpad technology,[79] bioimaging, optical MEMS and so on.

© 2015 WILEY-VCH Verlag GmbH & Co. KGaA, Weinheim

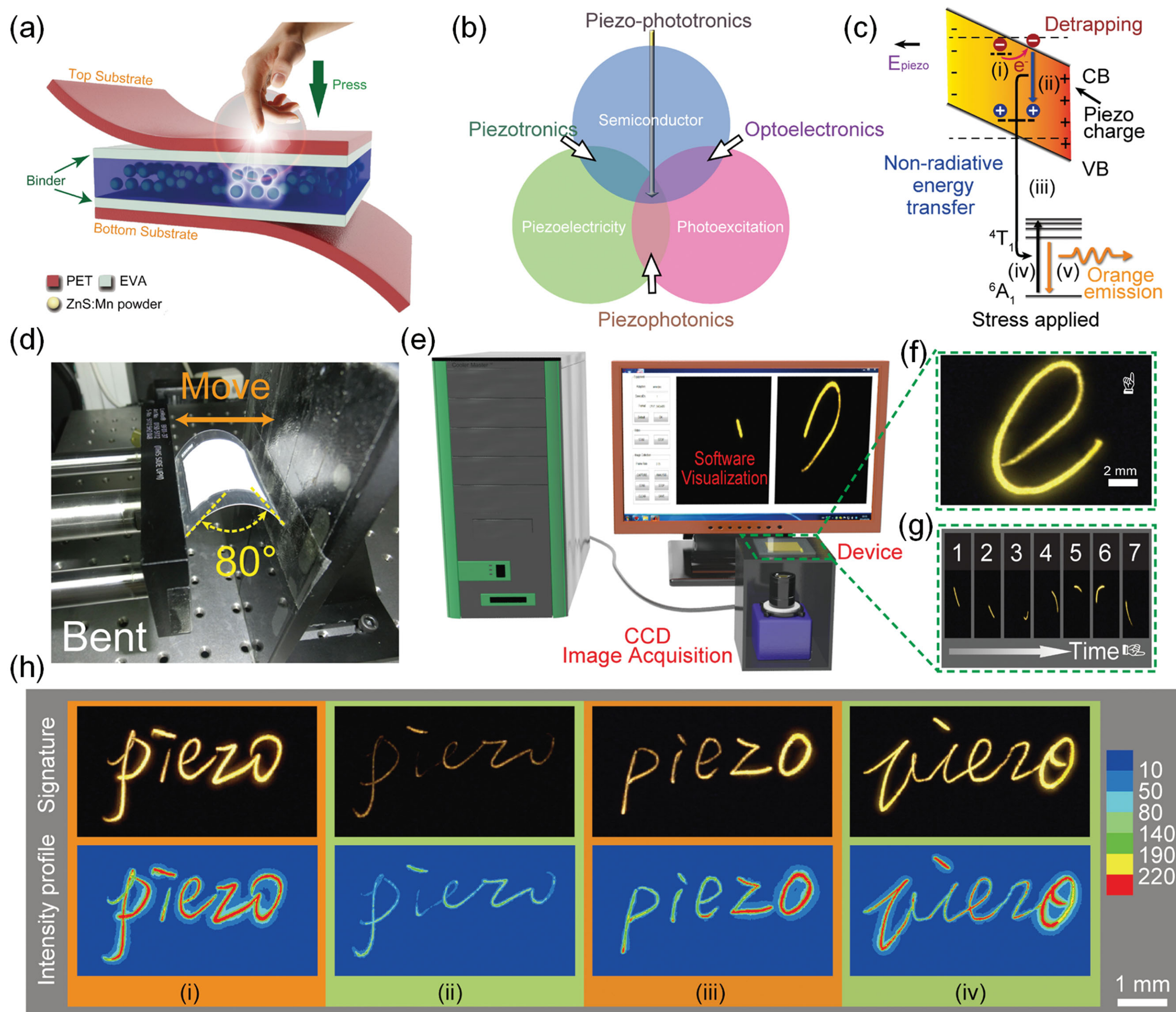

Figure 13. Dynamic pressure mapping the mechanoluminescence process. a) Schematic configuration of pressure-sensor matrix (PSM) devices. b) Schematic diagram showing the field of piezotronics, optoelectronics, piezo-phototronics, and piezophotonics. c) The piezo-photonic effect initiated the ML process. d) Flexibility test of PSM devices (0.5 g ZMPs, 0.1 mm-thick PET films). e–g) Schematic illustration of the image acquisition and processing system. f) Visualization of dynamic pressure distributions generated from a handwritten "e". g) Consecutive frames extracted from the dynamically capture video of the signing process based on an 80 ms time interval. h) Demonstrations of recording the signing habits of four signees by PSM devices. Pressure evenly distributed to every point during the signing process, with strong force (i); pressure evenly distributed to every point during the signing process, with weak force (ii); more pressures applied at the end of the signing process (iii); more pressure applied at the end and some turning points of the signing process (iv). a–h) Reproduced with permission.[82] Copyright 2015, Wiley-VCH.

6. Dynamic Pressure-Distribution Mapping Based on the Mechanoluminescence Process

Piezo-phototronic-effect-enhanced LED technology provides a new perspective to make optoelectronic devices[80] multifunctional. LEDs have been closely related to visualized display approaches,[81] which require real-time lighting. Inspired by former studies, it is feasible to employ the piezo-photonic property of ZnS:Mn particles (ZMP). In this process, a direct conversion from mechanical stress into optical signal was realized, and we have also designed a pressure-sensitive visualizing device: a more rapid-response flexible pressure-sensor matrix (PSM) based on this.[82]

The schematic configuration shows the structural design and the basic light-emitting process responding to the applied mechanical signals (**Figure 13**a). The core of this mechanical sensing light emission is a piezoelectric-induced photon-emission process (piezo-photonic property, Figure 13b). When there are applied strains, the energy band of ZnS inclines due to the strain-induced piezopotential, thus the excitation of Mn^{2+} ions is enhanced, which promotes the excitation of electrons, and the following de-excitation then brings about the photon emission

© 2015 WILEY-VCH Verlag GmbH & Co. KGaA, Weinheim
Adv. Mater. **2015**,
DOI: 10.1002/adma.201503500

as yellow light, while the light intensity is positively correlated to applied pressure (Figure 13c). The flexibility of PSM devices (0.5 g ZMPs, 0.1 mm-thick PET films) was tested as shown in Figure 13d. Information in this stress-to-light conversion process could be obtained in less than 10 ms, making it a rapid responding opto-mechanical sensor. As shown in Figure 13e, a real-time record of a handwritten letter "e" was captured. Moreover, with the assistance of a home-made image acquisition and processing system, the sensor matrix can not only record a single-point sliding dynamic pressure in handwriting[84] for signee identification, but can also map 2D planar pressure distributions by extracting the emission intensity to plot in real time (Figure 13f). All these features make this piezo-photonic device one of the most promising candidates for rapid-response pressure-mapping e-skin systems. Piezo-photonic and piezo-phototronic controlled optoelectronic devices will play a more and more important role in optoelectronic industry.[47,85]

7. Summary and Outlook

In summary, by three-way coupling of piezoelectricity, semiconductor and photo-excitations, discrete devices with certain functions are integrated to develop multi-functional systems. Fundamental to these applications is the strain-induced piezopotential which is generated by polarization charges in the crystal. Through this property, carrier transport across junction barriers is modulated by applied strains, which enables a new approach to human-machine interface technologies. Among these novel applications are piezo-phototronic-tuned LEDs, whose light-emission intensity could be manipulated by stress applied to the devices. From single-nanowire LEDs to an array of devices, piezo-phototronic-effect-tuned LEDs have developed from individual pressure-sensitive devices into high-resolution imaging of pressure distributions. The material system has been extended to both organic materials and silicon, significantly pushing forward the study of piezo-phototronics. It can be connected to other interfacial effects and lead to new phenomena and novel applications. It is expected that this technology will bring revolutionary applications to multi-functional systems, human–electronics interfacing display, energy harvesting,[79a,86] and so on.

Acknowledgements

The authors are grateful for the support received from the "thousand talents" program for the pioneer researcher and the innovation team in China, the Presidential Funding of the Chinese Academy of Sciences, and the National Natural Science Foundation of China (No. 51272238, 21321062, 51432005 and 61405040), the U.S. Department of Energy, the Office of Basic Energy Sciences (Award DE-FG02–07ER46394), and the National Science Foundation (DMR-1505319).

Received: July 19, 2015
Revised: August 28, 2015
Published online:

[1] a) D. Son, J. Lee, S. Qiao, R. Ghaffari, J. Kim, J. E. Lee, C. Song, S. J. Kim, D. J. Lee, S. W. Jun, *Nat. Nanotechnol.* **2014**, *9*, 397; b) L. Kou, T. Huang, B. Zheng, Y. Han, X. Zhao, K. Gopalsamy, H. Sun, C. Gao, *Nat. Commun.* **2014**, *5*, 3754.
[2] R. Jelinek, *Drug Dev. Res.* **2000**, *50*, 497.
[3] I. F. Akyildiz, W. Su, Y. Sankarasubramaniam, E. Cayirci, *Computer Networks* **2002**, *38*, 393.
[4] V. V. Tuchin, *J. Laser Appl.* **1993**, *5*, 43.
[5] Y. Bae, S. Fukushima, A. Harada, K. Kataoka, *Angew. Chem. Int. Ed.* **2003**, *42*, 4640.
[6] a) Y. Qiu, K. Park, *Adv. Drug Delivery Rev.* **2012**, *64*, 49; b) S. Wang, L. Lin, Z. L. Wang, *Nano Energy* **2015**, *11*, 436.
[7] Y.-H. Lee, J.-S. Kim, J. Noh, I. Lee, H. J. Kim, S. Choi, J. Seo, S. Jeon, T.-S. Kim, J.-Y. Lee, *Nano Lett.* **2013**, *13*, 5753.
[8] Z. Zhong, Y. Fang, W. Lu, C. M. Lieber, *Nano Lett.* **2005**, *5*, 1143.
[9] G. Juška, K. Arlauskas, M. Viliūnas, J. Kočka, *Phys. Rev. Lett.* **2000**, *84*, 4946.
[10] a) W. M. Du, X. Han, L. Lin, M. X. Chen, X. Y. Li, C. F. Pan, Z. L. Wang, *Adv. Energy Mater.* **2014**, *4*; b) M. X. Chen, X. Y. Li, L. Lin, W. M. Du, X. Han, J. Zhu, C. F. Pan, Z. L. Wang, *Adv. Funct. Mater.* **2014**, *24*, 5059; c) C. B. Han, C. Zhang, X. H. Li, L. Zhang, T. Zhou, W. Hu, Z. L. Wang, *Nano Energy* **2014**, *9*, 325; d) L. Lin, Y. Hu, C. Xu, Y. Zhang, R. Zhang, X. Wen, Z. Lin Wang, *Nano Energy* **2013**, *2*, 75.
[11] a) Z. L. Wang, *Adv. Mater.* **2012**, *24*, 4632; b) W. Z. Wu, C. F. Pan, Y. Zhang, X. N. Wen, Z. L. Wang, *Nano Today* **2013**, *8*, 619; c) Z. L. Wang, R. S. Yang, J. Zhou, Y. Qin, C. Xu, Y. F. Hu, S. Xu, *Mat. Sci. Eng., R.* **2010**, *70*, 320; d) Z. L. Wang, *Nano Today* **2010**, *5*, 540.
[12] a) H. Chen, C. Jia, C. Zhang, Z. Wang, C. Liu, presented at *IEEE Int. Symp. on Circuits and Systems 2007 (ISCAS 2007)*, New Orleans, LA, USA, May 2007; b) K. K. Tseng, L. Wang, *Smart Mater. Struct.* **2004**, *13*, 1017; c) N. Izyumskaya, Y.-I. Alivov, S.-J. Cho, H. Morkoc, H. Lee, Y.-S. Kang, *Crit. Rev. Solid. State* **2007**, *32*, 111.
[13] G. Gautschi, *Piezoelectric Sensors*, Springer, New York, **2002**.
[14] Z. L. Wang, W. Wu, *Natl. Sci. Rev.* **2013**, *1*, 62.
[15] a) Y. Hu, Y. Zhang, Y. Chang, R. L. Snyder, Z. L. Wang, *ACS Nano* **2010**, *4*, 4220; b) Q. Yang, W. Wang, S. Xu, Z. L. Wang, *Nano Lett.* **2011**, *11*, 4012; c) Q. Yang, X. Guo, W. Wang, Y. Zhang, S. Xu, D. H. Lien, Z. L. Wang, *ACS Nano* **2010**, *4*, 6285.
[16] R. T. Tung, *Mater. Sci. Eng., R.* **2001**, *35*, 1.
[17] R. S. Muller, T. I. Kamins, M. Chan, P. K. Ko, *Device Electronics for Integrated Circuits (2nd Ed.)*, Wiley, New York, **1986**, p. 54.
[18] Z. L. Wang, *MRS Bull.* **2012**, *37*, 814.
[19] Z. L. Wang, *Piezotronics and Piezo-Phototronics*, Springer-Verlag, Berlin/Heidelberg, Germany **2012**, p. 105.
[20] Z. L. Wang, J. Song, *Science* **2006**, *312*, 242.
[21] Z. L. Wang, *Adv. Funct. Mater.* **2008**, *18*, 3553.
[22] a) Z. L. Wang, *Mater. Sci. Eng., R.* **2009**, *64*, 33; b) Z. L. Wang, R. Yang, J. Zhou, Y. Qin, C. Xu, Y. Hu, S. Xu, *Mater. Sci. Eng., R.* **2010**, *70*, 320.
[23] Z. Gao, J. Zhou, Y. Gu, P. Fei, Y. Hao, G. Bao, Z. L. Wang, *J. Appl. Phys.* **2009**, *105*, 113707.
[24] a) C. K. Jeong, K. I. Park, J. Ryu, G. T. Hwang, K. J. Lee, *Adv. Funct. Mater.* **2014**, *24*, 2620; b) K. Momeni, G. Odegard, R. Yassar, *J. Appl. Phys.* **2010**, *108*, 114303.
[25] L. J. Brillson, Y. Lu, *J. Appl. Phys.* **2011**, *109*, 121301.
[26] E. H. Rhoderick, R. Williams, *Metal-Semiconductor Contacts*, Clarendon Press, Oxford, UK **1988**.
[27] S. M. Sze, K. K. Ng, *Physics of Semiconductor Devices*, 3rd Edition, John Wiley & Sons, Hoboken, NJ, USA **2006**.
[28] C. R. Crowell, S. M. Sze, *Solid-State Electronics* **1966**, *9*, 1035.
[29] A. N. Morozovska, E. A. Eliseev, S. V. Svechnikov, A. D. Krutov, V. Y. Shur, A. Y. Borisevich, P. Maksymovych, S. V. Kalinin, *Phys. Rev., B* **2010**, *81*, 205308.
[30] W. Wu, Y. Wei, Z. L. Wang, *Adv. Mater.* **2010**, *22*, 4711.
[31] Q. Yang, Y. Wu, Y. Liu, C. Pan, Z. L. Wang, *Phys. Chem. Chem. Phys.* **2014**, *16*, 2790.

© 2015 WILEY-VCH Verlag GmbH & Co. KGaA, Weinheim

[32] a) C. Xu, C. F. Pan, Y. Liu, Z. L. Wang, *Nano Energy* **2012**, *1*, 259; b) X. Wen, W. Wu, Z. L. Wang, *Nano Energy* **2013**, *2*, 1093; c) H. C. Weerasinghe, F. Huang, Y.-B. Cheng, *Nano Energy* **2013**, *2*, 174.
[33] Z. Wang, R. Yu, X. Wen, Y. Liu, C. Pan, W. Wu, Z. L. Wang, *ACS Nano* **2014**, *8*, 12866.
[34] H. D. Espinosa, R. A. Bernal, M. Minary-Jolandan, *Adv. Mater.* **2012**, *24*, 4656.
[35] a) C. F. Pan, H. Wu, C. Wang, B. Wang, L. Zhang, Z. D. Cheng, P. Hu, W. Pan, Z. Y. Zhou, X. Yang, J. Zhu, *Adv. Mater.* **2008**, *20*, 1644; b) M. L. Que, W. X. Guo, X. J. Zhang, X. Y. Li, Q. L. Hua, L. Dong, C. F. Pan, *J. Mater. Chem., A* **2014**, *2*, 13661; c) X. Fang, C. Shen, M. Ge, J. Rong, Y. Liu, A. Zhang, F. Wei, C. Zhou, *Nano Energy* **2015**, *12*, 43.
[36] Y. Zhang, Z. L. Wang, *Adv. Mater.* **2012**, *24*, 4712.
[37] X. Wen, W. Wu, C. Pan, Y. Hu, Q. Yang, Z. L. Wang, *Nano Energy* **2014**.
[38] Y. Zhang, Y. Liu, Z. L. Wang, *Adv. Mater.* **2011**, *23*, 3004.
[39] Y. Liu, Q. Yang, Y. Zhang, Z. Yang, Z. L. Wang, *Adv. Mater.* **2012**, *24*, 1410.
[40] Y. Liu, S. Niu, Q. Yang, B. D. Klein, Y. S. Zhou, Z. L. Wang, *Adv. Mater.* **2014**, *26*, 7209.
[41] Z. W. Pan, Z. R. Dai, Z. L. Wang, *Science* **2001**, *291*, 1947.
[42] A. Janotti, C. G. Van de Walle, *Rep. Prog. Phys.* **2009**, *72*, 126501.
[43] C. Wu, A. Kahn, *J. Appl. Phys.* **1999**, *86*, 3209.
[44] S. N. Mohammad, A. Salvador, H. Morkoc, *Proc. IEEE* **1995**, *83*, 1306.
[45] X. Duan, Y. Huang, R. Agarwal, C. M. Lieber, *Nature* **2003**, *421*, 241.
[46] X. Duan, Y. Huang, Y. Cui, J. Wang, C. M. Lieber, *Nature* **2001**, *409*, 66.
[47] X. Wang, Z. Li, W. Xu, S. A. Kulkarni, S. K. Batabyal, S. Zhang, A. Cao, L. H. Wong, *Nano Energy* **2015**, *11*, 728.
[48] a) R. M. Yu, W. Z. Wu, C. F. Pan, Z. N. Wang, Y. Ding, Z. L. Wang, *Adv. Mater.* **2015**, *27*, 940; b) R. M. Yu, C. F. Pan, Z. L. Wang, *Energ. Environ. Sci.* **2013**, *6*, 494; c) R. M. Yu, C. F. Pan, Y. F. Hu, L. Li, H. F. Liu, W. Liu, S. Chua, D. Z. Chi, Z. L. Wang, *Nano Res.* **2013**, *6*, 758.
[49] A. Tsukazaki, A. Ohtomo, T. Onuma, M. Ohtani, T. Makino, M. Sumiya, K. Ohtani, S. F. Chichibu, S. Fuke, Y. Segawa, *Nat. Mater.* **2005**, *4*, 42.
[50] Y. I. Alivov, E. Kalinina, A. Cherenkov, D. C. Look, B. Ataev, A. Omaev, M. Chukichev, D. Bagnall, *Appl. Phys. Lett.* **2003**, *83*, 4719.
[51] a) R. M. Yu, C. F. Pan, J. Chen, G. Zhu, Z. L. Wang, *Adv. Funct. Mater.* **2013**, *23*, 5868; b) R. M. Yu, L. Dong, C. F. Pan, S. M. Niu, H. F. Liu, W. Liu, S. Chua, D. Z. Chi, Z. L. Wang, *Adv. Mater.* **2012**, *24*, 3532; c) Q. Yang, Y. P. Wu, Y. Liu, C. F. Pan, Z. L. Wang, *Phys. Chem. Chem. Phys.* **2014**, *16*, 2790.
[52] S. Xu, C. Xu, Y. Liu, Y. F. Hu, R. S. Yang, Q. Yang, J. H. Ryou, H. J. Kim, Z. Lochner, S. Choi, R. Dupuis, Z. L. Wang, *Adv. Mater.* **2010**, *22*, 4749.
[53] a) A. Ng, Y. Xi, Y. Hsu, A. Djuriši , W. Chan, S. Gwo, H. Tam, K. Cheah, P. Fong, H. Lui, *Nanotechnology* **2009**, *20*, 445201; b) H. Y. Xu, Y. C. Liu, Y. X. Liu, C. S. Xu, C. L. Shao, R. Mu, *Appl. Phys. B.* **2005**, *80*, 871.
[54] Y. I. Alivov, J. E. Van Nostrand, D. C. Look, M. V. Chukichev, B. M. Ataev, *Appl. Phys. Lett.* **2003**, *83*, 2943.
[55] Y. I. Alivov, Ü. Özgür, S. Doğan, C. Liu, Y. Moon, X. Gu, V. Avrutin, Y. Fu, H. Morkoç, *Solid-State Electron.* **2005**, *49*, 1693.
[56] a) C. F. Pan, S. M. Niu, Y. Ding, L. Dong, R. M. Yu, Y. Liu, G. Zhu, Z. L. Wang, *Nano Lett.* **2012**, *12*, 3302; b) Y. S. Zhou, K. Wang, W. H. Han, S. C. Rai, Y. Zhang, Y. Ding, C. F. Pan, F. Zhang, W. L. Zhou, Z. L. Wang, *ACS Nano* **2012**, *6*, 6478; c) L. Dong, S. M. Niu, C. F. Pan, R. M. Yu, Y. Zhang, Z. L. Wang, *Adv. Mater.* **2012**, *24*, 5470.
[57] C. F. Pan, L. Dong, G. Zhu, S. M. Niu, R. M. Yu, Q. Yang, Y. Liu, Z. L. Wang, *Nat. Photonics* **2013**, *7*, 752.
[58] S. Lee, S.-H. Bae, L. Lin, S. Ahn, C. Park, S.-W. Kim, S. N. Cha, Y. J. Park, Z. L. Wang, *Nano Energy* **2013**, *2*, 817.
[59] a) Y. G. Zhu, Y. Wang, Y. Shi, J. I. Wong, H. Y. Yang, *Nano Energy* **2014**, *3*, 46; b) C. F. Pan, Z. T. Li, W. X. Guo, J. Zhu, Z. L. Wang, *Angew. Chem. Int. Ed.* **2011**, *50*, 11192.
[60] V. Nguyen, R. Yang, *Nano Energy* **2013**, *2*, 604.
[61] a) H. Zhang, Y. Yang, T.-C. Hou, Y. Su, C. Hu, Z. L. Wang, *Nano Energy* **2013**, *2*, 1019; b) H. Zhang, Y. Yang, Y. Su, J. Chen, C. Hu, Z. Wu, Y. Liu, C. Ping Wong, Y. Bando, Z. L. Wang, *Nano Energy* **2013**, *2*, 693; c) R. Zhou, G. Hu, R. Yu, C. Pan, Z. L. Wang, *Nano Energy* **2015**, *12*, 588.
[62] M. Peng, Z. Li, C. Liu, Q. Zheng, X. Shi, M. Song, Y. Zhang, S. Du, J. Zhai, Z. L. Wang, *ACS Nano* **2015**, *9*, 3143.
[63] L. Mao, Q. Chen, Y. Li, Y. Li, J. Cai, W. Su, S. Bai, Y. Jin, C.-Q. Ma, Z. Cui, L. Chen, *Nano Energy* **2014**, *10*, 259.
[64] Q. Yang, Y. Liu, C. Pan, J. Chen, X. Wen, Z. L. Wang, *Nano Lett.* **2013**, *13*, 607.
[65] a) T.-C. Hou, Y. Yang, Z.-H. Lin, Y. Ding, C. Park, K. C. Pradel, L.-J. Chen, Z. Lin Wang, *Nano Energy* **2013**, *2*, 387; b) C. F. Pan, R. M. Yu, S. M. Niu, G. Zhu, Z. L. Wang, *ACS Nano* **2013**, *7*, 1803; c) G. F. Hu, R. R. Zhou, R. M. Yu, L. Dong, C. F. Pan, Z. L. Wang, *Nano Res.* **2014**, *7*, 1083.
[66] a) C. F. Pan, Y. Fang, H. Wu, M. Ahmad, Z. X. Luo, Q. A. Li, J. B. Xie, X. X. Yan, L. H. Wu, Z. L. Wang, J. Zhu, *Adv. Mater.* **2010**, *22*, 5388; b) D. Y. Kim, S. Lee, Z.-H. Lin, K. H. Choi, S. G. Doo, H. Chang, J.-Y. Leem, Z. L. Wang, S.-O. Kim, *Nano Energy* **2014**, *9*, 101.
[67] B. K. Sharma, N. Khare, S. Ahmad, *Solid State Commun.* **2009**, *149*, 771.
[68] C. Wang, R. Bao, K. Zhao, T. Zhang, L. Dong, C. Pan, *Nano Energy* **2014**.
[69] D.-H. Lee, D.-H. Park, S. Kim, S. Y. Lee, *Thin Solid Films* **2011**, *519*, 5658.
[70] R. Bao, C. Wang, L. Dong, R. Yu, K. Zhao, Z. L. Wang, C. Pan, *Adv. Funct. Mater.* **2015**, *25*, 2884.
[71] Y. Gao, Z. L. Wang, *Nano Lett.* **2007**, *7*, 2499.
[72] S. Lee, Y. Lee, J. Park, D. Choi, *Nano Energy* **2014**, *9*, 88.
[73] V. R. Almeida, C. A. Barrios, R. R. Panepucci, M. Lipson, *Nature* **2004**, *431*, 1081.
[74] T. Zhang, R. Liang, L. Dong, J. Wang, J. Xu, C. Pan, *Nano Res.* **2015**, *8*, 2676.
[75] C. F. Pan, Z. X. Luo, C. Xu, J. Luo, R. R. Liang, G. Zhu, W. Z. Wu, W. X. Guo, X. X. Yan, J. Xu, Z. L. Wang, J. Zhu, *ACS Nano* **2011**, *5*, 6629.
[76] X. Li, M. Chen, R. Yu, T. Zhang, D. Song, R. Liang, Q. Zhang, S. Cheng, L. Dong, A. Pan, Z. L. Wang, J. Zhu, C. Pan, *Adv. Mater.* **2015**, *27*, 4447.
[77] P. Ball, *Nature* **2001**, *409*, 974.
[78] a) G. Zhu, P. Bai, J. Chen, Z. Lin Wang, *Nano Energy* **2013**, *2*, 688; b) G. Zhu, J. Chen, Y. Liu, P. Bai, Y. S. Zhou, Q. S. Jing, C. F. Pan, Z. L. Wang, *Nano Lett.* **2013**, *13*, 2282; c) G. Zhu, Z. H. Lin, Q. S. Jing, P. Bai, C. F. Pan, Y. Yang, Y. S. Zhou, Z. L. Wang, *Nano Lett.* **2013**, *13*, 847.
[79] a) X.-S. Zhang, M.-D. Han, R.-X. Wang, B. Meng, F.-Y. Zhu, X.-M. Sun, W. Hu, W. Wang, Z.-H. Li, H.-X. Zhang, *Nano Energy* **2014**, *4*, 123; b) H. Jin, L. Zhou, C. L. Mak, H. Huang, W. M. Tang, H. L. W. Chan, *Nano Energy* **2015**, *11*, 662.
[80] Z. L. Wang, G. Zhu, Y. Yang, S. H. Wang, C. F. Pan, *Mater. Today* **2012**, *15*, 532.
[81] a) J. Zhong, Q. Zhong, F. Fan, Y. Zhang, S. Wang, B. Hu, Z. L. Wang, J. Zhou, *Nano Energy* **2013**, *2*, 491; b) Z. Pi, J. Zhang, C. Wen, Z.-b. Zhang, D. Wu, *Nano Energy* **2014**, *7*, 33.
[82] X. Wang, H. Zhang, R. Yu, L. Dong, D. Peng, A. Zhang, Y. Zhang, H. Liu, C. Pan, Z. L. Wang, *Adv. Mater.* **2015**, *27*, 2324.
[83] a) D. O. Olawale, T. Dickens, W. G. Sullivan, O. I. Okoli, J. O. Sobanjo, B. Wang, *J. Lumin.* **2011**, *131*, 1407; b) Y. Zhang, G. Gao, H. L. W. Chan, J. Dai, Y. Wang, J. Hao, *Adv. Mater.* **2012**, *24*, 1729.
[84] E. S. Nour, M. O. Sandberg, M. Willander, O. Nur, *Nano Energy* **2014**, *9*, 221.
[85] a) C. F. Pan, J. Luo, J. Zhu, *Nano Res.* **2011**, *4*, 1099; b) C. F. Pan, W. X. Guo, L. Dong, G. Zhu, Z. L. Wang, *Adv. Mater.* **2012**, *24*, 3356.
[86] a) T.-C. Hou, Y. Yang, H. Zhang, J. Chen, L.-J. Chen, Z. Lin Wang, *Nano Energy* **2013**, *2*, 856; b) W. Tang, B. Meng, H. X. Zhang, *Nano Energy* **2013**, *2*, 1164.

© 2015 WILEY-VCH Verlag GmbH & Co. KGaA, Weinheim
Adv. Mater. **2015**,
DOI: 10.1002/adma.201503500